Lower Extremity EMG-driven Modeling of Walking with Automated Adjustment of Musculoskeletal Geometry

Andrew J. Meyer[1], Carolynn Patten[2,3], and Benjamin J. Fregly[1*]

[1] Department of Mechanical & Aerospace Engineering, University of Florida, Gainesville, FL

[2]Department of Physical Therapy, University of Florida, Gainesville, FL

[3]Neural Control of Movement Lab, Malcom Randall VA Medical Center, Gainesville, FL

*Corresponding author: Benjamin J. Fregly

E-mail: fregly@ufl.edu (BJF)

Abstract

Neuromusculoskeletal disorders affecting walking ability are often difficult to manage, in part due to limited understanding of how a patient's lower extremity muscle excitations contribute to the patient's lower extremity joint moments. To assist in the study of these disorders, researchers have developed electromyography (EMG) driven neuromusculoskeletal models utilizing scaled generic musculoskeletal geometry. While these models can predict individual muscle contributions to lower extremity joint moments during walking, the accuracy of the predictions can be hindered by errors in the scaled geometry. This study presents a novel EMG-driven modeling method that automatically adjusts surrogate representations of the patient's musculoskeletal geometry to improve prediction of lower extremity joint moments during walking. In addition to commonly adjusted neuromusculoskeletal model parameters, the proposed method adjusts model parameters defining muscle-tendon lengths, velocities, and moment arms. We evaluated our EMG-driven modeling method using data collected from a high-functioning hemiparetic subject walking on an instrumented treadmill at speeds ranging from 0.4 to 0.8 m/s. EMG-driven model parameter values were calibrated to match inverse dynamic moments for five degrees of freedom in each leg while keeping musculoskeletal geometry close to that of an initial scaled musculoskeletal model. We found that our EMG-driven modeling method incorporating automated adjustment of musculoskeletal geometry predicted net joint moments during walking more accurately than did the same method without geometric adjustments. Geometric adjustments improved moment prediction errors by 25% on average and up to 52%, with the largest improvements occurring at the hip. Predicted adjustments to musculoskeletal geometry were comparable to errors reported in the literature between scaled generic geometric models and measurements made from imaging data. Our results demonstrate that with appropriate experimental data, joint moment predictions for walking generated by

1 an EMG-driven model can be improved significantly when automated adjustment of musculoskeletal
2 geometry is included in the model calibration process.

Introduction

Neuromusculoskeletal disorders such as cerebral palsy [1], stroke [2], Parkinson's disease [3], and osteoarthritis [4] hinder walking ability and decrease quality of life for millions of people. Rehabilitation treatments have been developed to attempt to improve the walking ability of individuals with these disorders. However, the effectiveness of these treatments can vary between patients, in part due to the use of treatment design methods based more on subjective than objective methods [5]. For instance, for medial knee osteoarthritis, recent studies using instrumented knee implants found that gait modifications expected to reduced medial knee contact force [6–8] did not always do so [9,10]. Similarly, stroke rehabilitation methods that are effective for some patients may be ineffective for others [11]. Thus, treatment outcomes for neuromusculoskeletal disorders could potentially be improved through the use of more objective treatment design methods.

To assist with the design of more effective interventions, researchers have developed neuromusculoskeletal models of individual patients. A major challenge in neuromusculoskeletal modeling is determining how muscles contribute to net joint moments. Some studies have used electromyography (EMG) data with [12–19] and without [20–24] geometric musculoskeletal models to estimate the joint moments generated by muscles during movement. When geometric models are used, EMG-driven models predict net joint moments in three steps. First, muscle activation is determined from EMG data using a first or second order activation dynamics model [12,25]. Next, muscle force is determined from muscle activation and muscle-tendon kinematics using Hill-type muscle models [26,27]. Finally, joint moments are determined by combining estimated muscle forces with calculated muscle moment arms, which requires geometric modeling of muscle-tendon origins, insertions, and lines of action around bones and other muscles. Parameter values in activation dynamics models (e.g., activation and deactivation time constants, electromechanical time delay) and Hill-type muscle-tendon

models (e.g., optimal muscle fiber length, tendon slack length, peak isometric strength, pennation angle) are either taken directly from the literature [28] or calibrated via optimization to match experimental joint moments as closely as possible [12,14–16,29]. In contrast, muscle-tendon kinematics and muscle moment arm information needed for the last two steps is typically provided by a scaled generic musculoskeletal model. Unfortunately, several studies have demonstrated that scaled models may not represent the musculoskeletal geometry of individual subjects well [30–32]. Despite the presence of errors in muscle-tendon kinematics and moment arms in scaled geometric models, no study to date has attempted to adjust these quantities automatically to improve the prediction of net joint moments from EMG data.

This paper presents a novel EMG-driven modeling method that calibrates not only activation dynamics and muscle-tendon model parameter values but also geometric musculoskeletal model parameter values to patient walking data. The method was developed and evaluated using instrumented treadmill walking data collected from a high-functioning hemiparetic subject walking at five different speeds. Surrogate models of muscle-tendon length, velocity, and moment arms for each muscle were fitted as functions of joint angles [33,34] to data sampled from a scaled generic OpenSim [35] musculoskeletal model [36]. Surrogate model parameter values, along with activation dynamics and Hill-type muscle-tendon model parameter values, were adjusted via optimization such that lower extremity joint moments calculated from the subject's EMG data matched the subject's inverse dynamic joint moments from walking as closely as possible. Parameter values were adjusted for 35 muscles in each leg of the subject's model to match the hip flexion-extension (FE), hip adduction-abduction (AA), knee flexion-extension (FE), ankle plantar-dorsiflexion (PDF), and ankle inversion-eversion (IE) moments during treadmill walking. Calibrated EMG-driven models were evaluated by predicting joint

moments for walking trials withheld from calibration, including trials performed at faster non-calibration walking speeds.

Methods

Experimental Data

To support development and evaluation of our proposed EMG-driven modeling method, we collected experimental walking data from a single high-functioning hemiparetic male subject. All experimental procedures were approved by the University of Florida Health Science Center Institutional Review Board (IRB-01), and the subject provided written informed consent prior to participation. Motion capture (Vicon Corp., Oxford, UK), ground reaction (Bertec Corp., Columbus, OH), and EMG (Motion Lab Systems, Baton Rouge, LA) data were collected simultaneously while the subject walked on a split-belt instrumented treadmill (Bertec Corp., Columbus, OH) at five different speeds: 0.4, 0.5, 0.6, 0.7, and 0.8 m/s which included his preferred speed of 0.5 m/s. Motion capture data were recorded at a frequency of 100 Hz, and analog data were recorded at a frequency of 1000 Hz. More than 50 gait cycles were recorded for each walking speed. A static standing trial was also collected. The motion capture data were obtained using a modified Cleveland clinic marker set with additional markers added to the feet [37]. Ground reaction and marker motion data were filtered at a variable cut-off frequency of 7/tf Hz, where tf is the period of the gait cycle being processed, using a fourth-order zero phase lag Butterworth filter [38]. This variable cut-off frequency would cause data collected at a normal walking speed to be filtered at approximately 6 Hz.

EMG data were collected and processed for 16 muscles in each leg. These data used a combination of surface and fine-wire electrodes. Electrodes were placed following the SENIAM convention for surface electrodes [39] and the Delagi et al. Anatomical Guide for the Electromyographer for fine wire

electrodes [40]. Surface EMG data were collected for gluteus maximus and medius, semimembranosus, biceps femoris long head, rectus femoris, vastus medialis and lateralis, medial gastrocnemius, tibialis anterior, peroneus longus, and soleus. Fine-wire EMG data were collected for adductor longus, iliopsoas, tibialis posterior, flexor digitorum longus, and extensor digitorum longus. EMG data were high-pass filtered at 40 Hz [12], demeaned, rectified, and then low-pass filtered at a variable cut-off frequency 3.5/tf Hz. Filtering was performed using a fourth-order zero phase lag Butterworth filter. EMG data from each muscle were normalized to the maximum value over all trials and resampled to 101 time points per gait cycle while keeping an additional 20 time points before the start of the cycle to permit modeling of electromechanical delay. In addition, each processed EMG signal was offset on a cycle-by-cycle basis so that the minimum value was zero.

Model Description

Our EMG-driven model uses a Hill-type muscle model with a rigid tendon along with automatically adjusted musculoskeletal geometry [41]. However, the necessary muscle-tendon lengths, velocities, and moment arms commonly obtained from a geometric musculoskeletal model are instead approximated by polynomial functions of model generalized coordinates and their first derivatives [33,34]. Each muscle's moment about a spanned joint is represented by the following equation:

$$M = r \cdot F_o^M \cdot \left[a(e(t-d)) \cdot f_\ell(\tilde{\ell}^M(t)) \cdot f_v(\tilde{v}^M(t)) + f_p(\tilde{\ell}^M(t)) \right] \cos\alpha$$
$$0 < a(t) < 1$$
$$0.3 < \tilde{\ell}^M(t) < 1.3 \qquad (1)$$
$$-1 < \tilde{v}^M(t) < 1$$

where M is the moment about a given joint produced by the muscle, r is the moment arm of the muscle about the spanned joint, F_o^M is the peak isometric force of the muscle, a is the muscle's

activation which is a function of processed experimental EMG data e, t is time, d is an electromechanical time delay, $\tilde{\ell}^M$ and $\tilde{v}^M$ are the normalized muscle fiber length and velocity, respectively, and α is the muscle pennation angle, which is assumed to remain constant to facilitate subsequent calibration of musculoskeletal geometry. Neglecting tendon compliance, $\tilde{\ell}^M$ and $\tilde{v}^M$ are calculated using the following equations:

$$\tilde{\ell}^M = \frac{\ell^{MT} - \ell_s^T}{\ell_o^M \cos\alpha} \tag{2}$$

$$\tilde{v}^M = \frac{v^{MT}}{10 \cdot \ell_o^M} \tag{3}$$

where ℓ^{MT} is muscle-tendon length, ℓ_o^M is the optimal fiber length, ℓ_s^T is the tendon slack length, and v^{MT} is muscle-tendon velocity. $f_\ell(\tilde{\ell}^M(t))$, $f_p(\tilde{\ell}^M(t))$, and $f_v(\tilde{v}^M(t))$ represent the normalized muscle active force-length, passive force-length, and force-velocity curves (Fig 1). In all, our Hill-type muscle model requires specification of five parameter values d, ℓ_o^M, ℓ_s^T, F_o^M, and α and four time varying quantities a, ℓ^{MT}, v^{MT}, and r. Methods for calculating these four time varying quantities are described below.

Fig. 1. Relevant curves for our Hill-type muscle and activation nonlinearization model. Left: Normalized active, passive, and total force-length curves. Middle: Normalized force-velocity curve. Right: Neural-to-muscle activation nonlinearization curves for minimum nonlinearization (curve parameter = 0) and maximum nonlinearization (curve parameter = 0.35).

Muscle activation is calculated using a first order differential equation that describes excitation e to neural activation u dynamics and a nonlinear function that describes neural activation u to muscle activation a [42]. Neural activation is calculated by solving the first order differential equation proposed by He *et al*. [25]:

$$\frac{du(t)}{dt} = (c_1 e(t-d) + c_2)(e(t-d) - u(t)) \tag{4}$$

where $e(t-d)$ is excitation (i.e., processed EMG data) and $u(t)$ is neural activation. The constants c_1 and c_2 are defined as:

$$c_1 = \frac{1}{\tau_{act}} - \frac{1}{\tau_{deact}} \tag{5}$$

$$c_2 = \frac{1}{\tau_{deact}} \tag{6}$$

where τ_{act} and τ_{deact} are muscle activation and deactivation time constants, respectively. These time constants are constrained to be proportional to each other such that $\tau_{deact} = 4\tau_{act}$ based on the ratio commonly reported in the literature [27,43–45]. This linear differential equation is solved recursively over all time frames by discretizing Eq. (4) at each time point using a high accuracy backward finite difference approximation, assuming neural activation at the first two time points equals time-delayed muscle excitation at these time points, and solving for the unknown neural activation at the current time point:

$$u_i = \frac{2\Delta t(c_1 e(t_i - d) + c_2)e(t_i - d) + 4u_{i-1} - u_{i-2}}{2\Delta t(c_1 e(t_i - d) + c_2) + 3} \tag{7}$$

where Δt is the selected time interval and *i* represents the time frame for which neural activation is to be found. The nonlinear relationship between neural activation *u* and muscle activation *a* at time frame *i* is modeled using the equation:

$$a_i = (1 - c_3)u_i + c_3\left[\frac{g_1}{g_2(u_i + g_3)^{g_4} + g_5} + 1\right] \tag{8}$$

where c_3 is a constant that can vary from 0 (linear) to 0.35 (highly nonlinear), and g_1 - g_5 are values determined by fitting published experimental data from isometric contractions [42]. Constant

coefficients g_1-g_5 have values of -7.623, 29.280, 0.884, 17.227, and 4.108. This activation nonlinearity equation is a simplified version of functions proposed previously [42].

The time varying quantities ℓ^{MT}, v^{MT}, and r are calculated using polynomial functions of the joint angles and velocities that share common coefficients [33,34]. For muscles that span a single degree of freedom (DOF), the muscle-tendon length is approximated using the cubic polynomial equation:

$$\ell^{MT}(t) = b_0 + b_1\theta + b_2\theta^2 + b_3\theta^3 \tag{9}$$

where ℓ^{MT} is muscle-tendon length, θ is joint angle, and b_0 through b_3 are constant coefficients. Muscle-tendon velocity v^{MT} can then be calculated using the first derivative with respect to time of Eq. (9):

$$v^{MT}(t) = \frac{d\ell^{MT}}{dt} = b_1\dot{\theta} + 2b_2\theta\dot{\theta} + 3b_3\theta^2\dot{\theta} \tag{10}$$

where $\dot{\theta}$ is the joint angular velocity. Similarly, the muscle-tendon moment arm can be calculated from equation (9) using a relationship from An et al. [46]:

$$r(t) = -\frac{\partial\ell^{MT}}{\partial\theta} = -b_1 - 2b_2\theta - 3b_3\theta^2 \tag{11}$$

The negative sign in this expression is needed for consistency with our musculoskeletal modeling environment (see below). For muscles that span two DOFs, these equations are extended as follows:

$$\ell^{MT} = b_0 + b_1\theta_1 + b_2\theta_2 + b_3\theta_1\theta_2 + b_4\theta_1^2 + b_5\theta_2^2 + b_6\theta_1^2\theta_2 + b_7\theta_1\theta_2^2 + b_8\theta_1^3 + b_9\theta_2^3 \tag{12}$$

$$\begin{aligned} v^{MT} = {} & b_1\dot{\theta}_1 + b_2\dot{\theta}_2 + b_3(\dot{\theta}_1\theta_2 + \theta_1\dot{\theta}_2) + 2b_4\theta_1\dot{\theta}_1 + 2b_5\theta_2\dot{\theta}_2 + \ldots \\ & b_6(2\theta_1\dot{\theta}_1\theta_2 + \theta_1^2\dot{\theta}_2) + b_7(\dot{\theta}_1\theta_2^2 + 2\theta_1\theta_2\dot{\theta}_2) + 3b_8\theta_1^2\dot{\theta}_1 + 3b_9\theta_2^2\dot{\theta}_2 \end{aligned} \tag{13}$$

$$r_1 = -\frac{\partial\ell^{MT}}{\partial\theta_1} = -b_1 - b_3\theta_2 - 2b_4\theta_1 - 2b_6\theta_1\theta_2 - b_7\theta_2^2 - 3b_8\theta_1^2 \tag{14}$$

$$r_2 = -\frac{\partial \ell^{MT}}{\partial \theta_2} = -b_2 - b_3\theta_1 - 2b_5\theta_2 - b_6\theta_1^2 - 2b_7\theta_1\theta_2 - 3b_9{\theta_2}^2 \quad (15)$$

For muscles that span three or four DOFs, Eqs. (9), (10), and (11) are extended in a similar manner by adding terms corresponding to the additional joint angles and velocities. These polynomial functions can be viewed as surrogate models of muscle-tendon lengths, velocities, and moment arms.

Model Calibration

In our EMG-driven model calibration process, we start with a generic full-body OpenSim musculoskeletal model [35]. The authors of that study created this initial model using measurements made on 21 cadaveric specimens. Since the present study focuses on lower limb motion during walking, the generic model was reduced to 29 DOFs by removing toes, forearm, and wrist DOFs. The lower extremity joints were modeled as follows: the hips as ball-and-socket joints, the knees as hinge joints (flexion/extension) with prescribed translations defined as a function of knee rotation [47], and the ankles as two non-intersecting hinge joints. After removal of muscles without related EMG signals, 35 muscles remained whose names, functions, and excitation groups are listed in Table 1. Many of these muscles represented compartments of larger muscles that were split to model their function more accurately. For instance, gluteus maximus was split into three compartments modeled as individual muscles with a common excitation signal.

Table 1: List of muscles in the model, which DOF each muscle actuates, and source of each muscle's excitation signal.

Muscle	Actuates	EMG Signal Source	EMG Type
Adductor brevis	Hip FE, Hip AA	Adductor longus	Fine wire
Adductor longus	Hip FE, Hip AA		
Adductor magnus distal	Hip FE, Hip AA		
Adductor magnus ischial	Hip FE, Hip AA		
Adductor magnus middle	Hip FE, Hip AA		
Adductor magnus proximal	Hip FE, Hip AA		

Gluteus maximus superior	Hip FE, Hip AA	Gluteus maximus	Surface
Gluteus maximus middle	Hip FE, Hip AA		
Gluteus maximus inferior	Hip FE, Hip AA		
Gluteus medius anterior	Hip FE, Hip AA	Gluteus medius	Surface
Gluteus medius middle	Hip FE, Hip AA		
Gluteus medius posterior	Hip FE, Hip AA		
Gluteus minimus anterior	Hip FE, Hip AA		
Gluteus minimus middle	Hip FE, Hip AA		
Gluteus minimus posterior	Hip FE, Hip AA		
Iliacus	Hip FE, Hip AA	Iliacus or Psoas	Fine wire
Psoas	Hip FE, Hip AA		
Semimembranosus	Hip FE, Hip AA, Knee FE	Semimembranosus	Surface
Semitendinosus	Hip FE, Hip AA, Knee FE		
Biceps femoris long head	Hip FE, Hip AA, Knee FE	Biceps femoris long head	Surface
Biceps femoris short head	Knee FE		
Rectus femoris	Hip FE, Hip AA, Knee FE	Rectus femoris	Surface
Vastus medialis	Knee FE	Vastus medialis	Surface
Vastus intermedius	Knee FE		
Vastus lateralis	Knee FE	Vastus lateralis	Surface
Lateral gastrocnemius	Knee FE, Ankle PDF, Ankle IE	Medial gastrocnemius	Surface
Medial gastrocnemius	Knee FE, Ankle PDF, Ankle IE		
Tibialis anterior	Ankle PDF, Ankle IE	Tibialis anterior	Surface
Tibialis posterior	Ankle PDF, Ankle IE	Tibialis posterior	Fine wire
Peroneus brevis	Ankle PDF, Ankle IE	Peroneus longus	Surface
Peroneus longus	Ankle PDF, Ankle IE		
Peroneus tertius	Ankle PDF, Ankle IE		
Soleus	Ankle PDF, Ankle IE	Soleus	Surface
Extensor digitorum longus	Ankle PDF, Ankle IE	Extensor digitorum longus	Fine wire
Flexor digitorum Longus	Ankle PDF, Ankle IE	Flexor digitorum longus	Fine wire

The first step in our EMG-driven model calibration process was scaling of the generic musculoskeletal model in OpenSim to match static trial marker data. Each segment's scale factors were based on the ratio of distances between markers placed over bony landmarks and distances between corresponding markers in the generic model. Symmetry was maintained between the right and left sides of the body. The following segments were scaled: pelvis, torso, upper arms, forearms, thighs, shanks, and feet.

Following scaling, the next step was calibration of lower extremity joint positions and orientations and of marker positions within the body segments such that an OpenSim inverse kinematics analysis matched measured marker locations during walking as closely as possible [37,48]. This calibration step was performed in MATLAB via nonlinear least squares optimization and the OpenSim MATLAB application programming interface for performing repeated inverse kinematic analyses. A single representative walking trial at 0.5 m/s, the subject's preferred walking speed, was used for this purpose. Distances between pairs of markers within the same body segment were fixed during calibration. Joint positions and orientations within the body segments were adjusted only for the lower extremities while marker positions within the body segments were adjusted for all segments except the arms. Since relocating joint centers causes segment lengths to change, the model geometry was rescaled based on the new joint-to-joint distances. Model symmetry was maintained between the right and left sides during this calibration step.

Given the scaled musculoskeletal model with calibrated joint parameters, the third step of the calibration process was creation of surrogate models of muscle-tendon geometry using Eqs. (9)-(15) [33,34]. Each muscle's muscle-tendon length and moment arms were calculated by an OpenSim muscle analysis for 1000 different model poses specified using Latin hypercube sampling over a wide range of joint angles that went well beyond those that occur during walking. Surrogate models of muscle-tendon lengths and moment arms were then fitted simultaneously by calculating model coefficients using linear least squares regression. Muscle-tendon velocities were not matched because the sampling process was time independent. The resulting surrogate geometric models closely reproduced the subject's muscle-tendon lengths, velocities, and moment arms for walking as calculated by the scaled OpenSim musculoskeletal model with calibrated joint parameters. Median fitting errors for all muscles were less than 1.6 mm for moment arms and 0.69 mm for muscle-tendon lengths.

The final step of the calibration process was creation of an EMG-driven model by optimizing activation, Hill-type muscle-tendon, and surrogate geometric model parameter values for all muscles such that lower extremity joint moments predicted by the model matched those calculated by inverse dynamics as closely as possible (Fig. 2). The design variables altered by the optimization were: electromechanical delays d, activation time constants τ_{act}, activation nonlinearity constants c_3, scale factors defining the maximum processed EMG value achievable by each muscle, common scale factors for the optimal muscle fiber length and tendon slack length of each muscle, and coefficients b_0 through b_n defining muscle-tendon lengths, velocities, and moment arms. These model parameter values were calibrated using a sequence of seven optimizations to reduce the likelihood of entrapment in a local minimum. In the first and fourth optimizations, electromechanical delays, muscle activation time constants, activation nonlinearity constants, and EMG scale factors were adjusted while all other design variables were fixed at their initial or previous values. In the second and fifth optimizations, common scale factors for optimal muscle fiber lengths and tendon slack lengths were adjusted. In the third and sixth optimizations, coefficients defining muscle-tendon geometry were adjusted. Finally, in the seventh optimization, all design variables were adjusted simultaneously. All optimizations were performed using MATLAB's fmincon sequential quadratic programming algorithm.

Fig. 2. Flowchart of EMG-driven model calibration process for walking. The goal is to find model parameter values (i.e., activation parameters, surrogate geometry parameters, and muscle-tendon parameters) such that experimental processed EMG data and joint kinematics can be input to the model and lower extremity joint moments that closely match experimental joint moments are output from the model. Blue lines indicate model parameter values changed by the optimization process.

To maintain anatomic realism, the cost function for these optimizations not only minimized errors in model-predicted lower extremity joint moments but also penalized changes in model parameter values, muscle kinematics, and muscle moment arms away from their initial values and trajectories [48]. Joint

moment errors were calculated for both active and passive moments. Active moments were calculated from the subject's walking data via an OpenSim inverse dynamic analysis performed for ten gait cycles from each walking speed. Passive moments were taken from measurements reported in the literature for a wide range of joint angle combinations [49]. These passive moment data were included to provide additional information for estimating passive muscle-tendon properties. Initial model parameter values were either taken directly from the literature or customized to the subject based on information in the literature (for example, peak isometric force values were calculated using information reported in [50]), while initial muscle kinematic and moment arm trajectories were taken from the subject's scaled OpenSim model. Details regarding specification of initial guesses, variable bounds, and cost function terms can be found in the Appendix.

Model Evaluation

Using the optimization process described above, we evaluated our EMG-driven modeling process by performing two "calibrate, then test" scenarios. Gait cycles from all walking speeds were selected for this process. To develop the necessary inputs for calibration and testing, we performed OpenSim inverse kinematic and inverse dynamic analyses for each walking cycle. Using the inverse kinematic results, we generated reference muscle-tendon length, velocity, and moment arm curves from the surrogate geometric models, which avoided potential discontinuities caused by problems associated with muscle wrapping surfaces. All EMG, inverse kinematic, inverse dynamic, and muscle-tendon geometric curves were resampled to 101 time points per walking cycle. In addition, to prevent numerical issues at heel strike and toe off, and to accommodate identification of electromechanical delays, we included 20 additional time frames of all data before the start of each gait cycle. Given the curves output by OpenSim analyses, we identified and removed outlier trials using criteria described in the Appendix.

The two "calibrate, then test" evaluation scenarios differed based on whether or not the testing phase included walking data from faster speeds not included in the calibration phase. For the first scenario, model calibration was performed using 50 trials of data from all five walking speeds (10 trials per speed) and model testing was performed using an additional 50 trials of data from the same five speeds. For the second scenario, model calibration was performed using 30 trials of data from the three slowest walking speeds (10 trials per speed) and model testing was performing using an additional 50 trials of data from all five walking speeds, including 0.7 and 0.8 m/s. For both scenarios, two EMG-driven models, one with and one without geometric adjustments, were calibrated via optimization to match inverse dynamic joint moment data from the calibration walking trials. All models were adjusted to match joint moments for five DOFs in each leg: hip flexion extension, hip adduction-abduction, knee flexion-extension, ankle plantar-dorsiflexion, and ankle inversion-eversion. Since EMG data were collected from only 16 muscles in each leg, excitations for muscles without EMG data were specified using EMG data from related muscles [14]. A list of the muscles used in the model, the associated joints they actuate, and the EMG signals that control them can be found in Table 1. Using only joint kinematics and processed EMG signals as inputs, the calibrated EMG-driven models were used to predict joint moments at each speed for 10 walking trials withheld from calibration. Mean absolute errors (MAE) between predicted and inverse dynamic joint moments were calculated to evaluate the accuracy of all EMG-driven models:

$$\mathrm{MAE} = \frac{1}{n}\sum_{i=1}^{n} | M_i^{ID} - M_i^{EtM} | \tag{16}$$

where M_i^{ID} is a moment from inverse dynamics, M_i^{EtM} is the corresponding moment predicted by an EMG-driven model, and n is the number of time frames being evaluated.

Results

When calibrated using walking data from all five speeds, the EMG-driven model with geometric adjustments (henceforth the "WGA model") produced more accurate moment predictions for all joints than did the model without geometric adjustments (henceforth the "NGA model") (Figs. 3 and 4, Table 2). For additional walking trials not used in the calibration process, geometric adjustments improved joint moment predictions by an average of 25%, with the largest improvements occurring at the hip (33%), following by the ankle (21%), and finally the knee (16%). The largest average improvement for any joint moment occurred for hip adduction-abduction (42%). Improvements produced by adding geometric adjustments were generally comparable between legs and across walking speeds.

When calibrated using walking data from only the three slowest speeds, the WGA model again produced more accurate moment predictions for all joints than did the NGA model, with the one exception being the right ankle inversion-eversion moment (Figs. 5 and 6, Table 3). For additional walking trials at speeds used in the calibration process, geometric adjustments improved joint moment predictions by an average of 23%, with the largest improvements occurring at the hip (34%), following by the knee (22%), and finally the ankle (12%). The largest average improvement for any joint moment occurred for hip adduction-abduction (43%). For additional walking trials at faster speeds not used for calibration, geometric adjustments improved joint moment predictions by an average of 15%, with the largest improvements again occurring at the hip (23%), following by the ankle (10%), and finally the knee (9%). The largest average improvement for any joint moment again occurred for hip adduction-abduction (36%). As noted above, the one exception was the right ankle inversion-eversion moment, which exhibited worse moment predictions (9% of an extremely small moment) with the addition of geometric adjustments.

Table 2: MAE values for testing trials using EMG-driven models without (NGA) and with (WGA) geometric adjustments calibrated using all walking speeds. The percent change in MAE when geometric adjustments were added is also reported.

Gait Speed	Model Type	Hip FE (N-m)		Hip AA (N-m)		Knee FE (N-m)		Ankle PDF (N-m)		Ankle IE (N-m)	
		Right	Left	Right	Left	Right	Left	Right	Left	Right	Left
0.4 m/s	NGA	5.28	5.31	7.23	7.91	6.60	5.43	7.44	5.96	2.48	6.18
	WGA	3.83	4.61	3.58	4.99	5.22	4.69	5.44	5.28	2.27	4.88
	% Change	-27.43	-13.19	-50.46	-36.92	-20.93	-13.71	-26.96	-11.43	-8.54	-21.09
0.5 m/s	NGA	4.23	5.94	5.87	7.64	7.07	4.67	7.50	7.14	3.52	5.74
	WGA	3.47	4.47	4.02	4.26	5.33	4.28	4.85	6.09	3.46	4.40
	% Change	-18.06	-24.69	-31.49	-44.30	-24.62	-8.26	-35.31	-14.70	-1.90	-23.43
0.6 m/s	NGA	5.46	6.76	8.01	7.81	5.33	5.11	7.27	7.24	3.42	5.98
	WGA	4.10	4.94	4.55	4.46	4.27	4.81	4.89	5.63	2.84	4.27
	% Change	-24.91	-27.00	-43.23	-42.92	-19.91	-5.78	-32.76	-22.21	-17.04	-28.53
0.7 m/s	NGA	6.33	7.08	6.87	8.26	5.52	6.05	8.01	7.43	3.15	5.78
	WGA	4.73	5.50	4.41	4.46	4.55	4.92	5.98	5.51	2.95	4.05
	% Change	-25.34	-22.22	-35.88	-45.98	-17.50	-18.58	-25.34	-25.85	-6.23	-30.02
0.8 m/s	NGA	6.92	7.45	7.17	8.81	6.43	4.76	8.48	7.24	3.56	5.50
	WGA	5.11	5.04	4.55	4.79	5.28	4.22	5.93	5.99	2.91	4.22
	% Change	-26.17	-32.32	-36.50	-45.61	-17.90	-11.31	-30.11	-17.29	-18.15	-23.38
Average	NGA	5.65	6.51	7.03	8.09	6.19	5.20	7.74	7.00	3.23	5.84
	WGA	4.25	4.91	4.22	4.59	4.93	4.58	5.42	5.70	2.88	4.36
	% Change	-24.76	-24.50	-39.95	-43.22	-20.36	-11.87	-30.02	-18.60	-10.56	-25.27

1

Table 3: MAE values for testing trials using EMG-driven models without (NGA) and with (WGA) geometric adjustments calibrated using only the three slowest walking speeds. The percent change in MAE when geometric adjustments were added is also reported. Row headers marked with a * indicate walking speeds not included in the calibration process.

Gait Speed	Model Type	Hip FE (N-m)		Hip AA (N-m)		Knee FE (N-m)		Ankle PDF (N-m)		Ankle IE (N-m)	
		Right	Left	Right	Left	Right	Left	Right	Left	Right	Left
0.4 m/s	NGA	5.06	5.13	6.98	7.77	6.69	5.34	7.25	5.06	2.01	5.82
	WGA	3.78	4.45	3.37	4.99	4.37	4.50	5.79	4.80	2.07	4.60
	% Change	-25.21	-13.30	-51.67	-35.77	-34.68	-15.69	-20.22	-5.08	2.96	-20.88

0.5 m/s	NGA	4.32	5.77	6.41	7.38	7.24	4.47	6.80	6.02	2.88	5.29
	WGA	3.15	4.20	3.57	4.21	4.18	3.93	4.89	5.56	3.50	4.00
	% Change	-26.96	-27.25	-44.28	-42.92	-42.26	-12.12	-28.07	-7.72	21.55	-24.41
0.6 m/s	NGA	5.54	6.64	8.26	7.70	6.39	5.68	6.74	5.79	2.70	5.53
	WGA	4.30	4.76	4.71	4.39	5.88	4.84	5.23	5.30	2.70	3.83
	% Change	-22.43	-28.41	-42.95	-43.00	-7.97	-14.77	-22.41	-8.47	-0.14	-30.70
Average	NGA	4.97	5.85	7.22	7.62	6.77	5.17	6.93	5.62	2.53	5.55
	WGA	3.75	4.47	3.89	4.53	4.81	4.43	5.30	5.22	2.76	4.14
	% Change	-24.68	-23.61	-46.16	-40.51	-28.99	-14.32	-23.49	-7.19	8.90	-25.27
*0.7 m/s	NGA	6.50	7.38	7.42	8.13	6.26	7.27	7.66	6.45	2.46	5.29
	WGA	5.14	6.70	4.67	5.21	6.23	6.12	6.18	5.93	2.95	3.73
	% Change	-20.93	-9.30	-37.02	-35.97	-0.46	-15.84	-19.29	-8.01	20.23	-29.48
*0.8 m/s	NGA	7.02	7.42	7.50	9.40	7.75	6.75	8.03	6.63	2.95	5.19
	WGA	6.25	7.34	4.89	5.84	7.52	5.65	6.45	6.54	2.92	4.08
	% Change	-10.93	-1.06	-34.79	-37.87	-2.91	-16.35	-19.74	-1.41	-1.17	-21.32
*Average	NGA	6.76	7.40	7.46	8.76	7.01	7.01	7.85	6.54	2.70	5.24
	WGA	5.69	7.02	4.78	5.52	6.88	5.89	6.32	6.23	2.94	3.91
	% Change	-15.74	-5.17	-35.90	-36.99	-1.81	-16.09	-19.52	-4.66	8.55	-25.44

Fig. 3. Average joint moment predictions for walking at 0.5 m/s when calibrating using all five walking speeds. NGA stands for no geometric adjustments and WGA stands for with geometric adjustments. Average values were calculated at each time point after each gait cycle was resampled to 101 points.

Fig. 4. Average joint moment predictions for walking at 0.8 m/s when calibrating using all five walking speeds. NGA stands for no geometric adjustments and WGA stands for with geometric adjustments. Average values were calculated at each time point after each gait cycle was resampled to 101 points.

Fig. 5. Average joint moment predictions for walking at 0.5 m/s when calibrating using only the three slowest walking speeds. NGA stands for no geometric adjustments and WGA stands for with geometric adjustments. Average values were calculated at each time point after each gait cycle was resampled to 101 points.

Fig. 6. Average joint moment predictions for walking at 0.8 m/s when calibrating using only the three slowest walking speeds. NGA stands for no geometric adjustments and WGA stands for with geometric adjustments. Average values were calculated at each time point after each gait cycle was resampled to 101 points.

Geometric adjustments improved joint moment predictions by making relatively small changes to muscle-tendon lengths and moment arms (Tables A2 and A3 in the Appendix). For both "calibrate, then test" scenarios, the average change in muscle-tendon length was less than 0.9 cm (5%), while the average change in muscle moment arm was less than 0.5 cm (17%). On average, the largest muscle-tendon length change was 3.8 cm (8%) for the left semitendinosus muscle, the largest absolute mean moment arm change was 1.8 cm (44%) for the left soleus muscle about the left ankle joint, and the largest percent moment arm change was 121% (0.8 cm) for the left medial gastrocnemius muscle about the left subtalar joint. These changes allowed the WGA and NGA models to match the published passive moment curves well, though the WGA model matched them slightly better (Fig. 7).

Fig. 7. Passive Joint Moment Matching. Passive moments predicted by our EMG-driven models calibrated using all walking speeds (dashed lines) compared to published passive moments (solid lines) for the WGA and NGA models.

Discussion

This study evaluated a novel method for calibrating an EMG-driven model of walking, including automated adjustment of surrogate musculoskeletal geometry, to match experimental joint moment data. In addition to geometric adjustments, the method possesses several other unique features, including scaling of EMG signals and matching of published lower extremity passive joint moment curves. The approach was evaluated using walking data collected from a hemiparetic subject, highlighting that neurological impairment may not limit the potential utility of the approach (i.e., the subject's neural control strategy does not need to be "optimal"). When scaled generic musculoskeletal geometry was

used without adjustment, the EMG-driven model was less accurate at predicting joint moments, especially for the hip. Though we cannot claim that the adjusted geometry is a more accurate representation of the subject's actual geometry, these adjustments improved lower extremity joint moment predictions both for speeds used in the calibration process and for faster speeds omitted from calibration. When creating EMG-driven models of walking that include the hip, adjustments to musculoskeletal geometry may be especially helpful for improving the accuracy of hip moment predictions.

Our EMG-driven models with geometric adjustments predicted joint moments for walking more accurately and under more complex conditions than did previous EMG-driven studies that predicted joint moments using only walking data (Table 4) [13,15]. In our study, joint moment predictions were generated for five DOFs in both legs using 16 EMG signals per leg with a large number of walking trials collected at multiple walking speeds, including trials from faster walking speeds not included in the calibration process. In two previous EMG-driven studies that calibrated their models using only walking data, joint moments were predicted for only the ankle [13] or only the knee [15] using 7 to 10 EMG signals from a single leg with a small number of walking trials collected at a single walking speed. Despite the use of more complex conditions, our EMG-driven model still produced lower moment errors for walking speeds included in and omitted from calibration. The only EMG-driven modeling study to date to report errors in predicted hip moments during walking is Sartori et al. (2012) [14]. Though our hip moment prediction errors are much lower than those reported in that study (see Table 4), their single- and multi-DOF EMG-driven models were calibrated using data from walking plus three other activities, which likely have made their calibration process more difficult. At the same time, their high hip moment prediction errors are consistent with our findings that geometric adjustments are especially helpful for the hip.

Table 4: Comparison of moment error values reported in the literature with moment error values reported in this study. Other EMG-driven studies not indicated [12,16-19] have prediction errors greater than those listed in this table or use a variety of activities for calibration and/or testing and are therefore disqualified from comparison. For the knee and ankle joints, the studies shown calibrate and test their models using only gait data. Sartori et al. 2014 was the only available EMG-driven model of the hip, and was calibrated using a variety of activities.

	Literature		This Study Single-DOF		This Study Multi-DOF	
DOF	**Single-DOF**	**Multi-DOF**	**NGA**	**WGA**	**NGA**	**WGA**
Hip FE	17[1]	26[1]	4.42	3.87	6.08	4.58
Hip AA	9.7[1]	16[1]	6.39	4.02	7.56	4.41
Knee FE	7.80[2]	7.6[1]	4.61	4.27	5.70	4.76
Ankle PDF	6.03[3]	16[1]	6.51	4.70	7.37	5.56
Ankle IE	--	--	2.96	2.36	4.53	3.62

[1]Sartori *et al*. [14] MAE*, [2]Kumar *et al*. [15] RMSE, [3]Bogey *et al*. [13] RMSE
RMSE indicates root mean square error
*Values from Sartori *et al.* were estimated from figures since values for walking only were not explicitly stated.

Most studies calibrate their EMG-driven models to predict moments about a single DOF, which is a simpler problem than predicting moments about five DOFs simultaneously. Sartori *et al*. (2012) [14] found that single-DOF NGA models calibrated with similar accuracy as a four-DOF NGA model. In contrast, when we calibrated single-DOF NGA and WGA models using our optimization framework, moment errors were always lower than with the corresponding multi-DOF model (Table 4). This finding makes sense since multi-DOF models constrain the solution more than do single-DOF models due to inter-joint coupling caused by muscles that actuate multiple DOFs. Interestingly, our multi-DOF WGA model produced comparable moment errors (sometimes slightly better, sometimes slightly worse) to our single-DOF NGA models, again highlighting the value of adding geometric adjustments.

In addition to adjustment of surrogate musculoskeletal geometry, our EMG-driven modeling approach possessed six other unique features that likely improved our moment predictions even without geometric adjustments. First, our study utilized fine-wire EMG data from several deep muscles. Fine-wire EMG data allowed us to include potentially important muscles omitted from most other studies: iliopsoas, tibialis posterior, flexor digitorum longus, and extensor digitorum longus. Omission of these

muscles likely contributed to increased moment prediction errors in previous studies, especially omission of iliopsoas for the hip flexion moment. Secondly, our study filtered EMG data with a variable low pass cutoff frequency that depended on the period of the gait cycle. When using a constant low pass cutoff frequency, we found that slow gait speeds would have comparatively noisier EMG signals than did faster speeds, which adversely affected our moment predictions. In contrast, when a variable low pass cutoff frequency was used, moment predictions became more reliable across speeds. Third, our study optimized scale factors defining maximum EMG values. Most studies normalize EMG data to a maximum voluntary contraction trial (MVC) or the maximum EMG value over all collected trials. However, these methods may be unreliable indicators of maximum muscle excitation [51], and true MVC trials are often hard to obtain. Furthermore, maximal M-wave measurements demonstrate that MVC trials produce EMG values that are smaller than maximum EMG [51–53]. Therefore, we decided to optimize a muscle excitation scale factor and penalize it for deviating away from its initial value. Inclusion of optimized excitation scale factors was one of the most valuable unique additions in our approach. Fourth, our study included matching of experimentally measured passive joint moments reported in the literature [49]. These moments corresponded to much larger ranges and combinations of joint angles than occur during walking. Though these data were not subject specific, they likely helped the muscles in our model to traverse reasonable ranges on their normalized force-length curves. Matching of passive joint moment curves was another highly valuable unique addition in our approach. Fifth, our study used a larger number of walking trials for model calibration and testing. Use of a large number of trials allowed us to minimize the impact of outlier trials in both our calibration and testing process. It also allowed us to capture the broadest possible variability in the subject's walking data, which was important since our method uses only walking data for calibration. Lastly, our study included kinematic calibration of lower extremity joint centers and orientations [37,48]. Previous studies have

demonstrated that inverse dynamics moments are sensitive to the position and orientation of joint centers in the body segments [54]. As a result, the moments being matched during calibration may not be the true moments produced by muscles, resulting in EMG-driven calibration and prediction errors. Furthermore, placing a joint center in the wrong location causes offsets in muscle moment arms, further decreasing the quality of the moment predictions. Calibration of lower limb joint positions and orientations may have eliminated some of these modeling errors, thereby improving EMG-driven predictions.

While adjustments to geometric parameter values greatly reduced moment prediction errors, the accuracy with which the adjusted geometry represents the subject is unknown. Scaled generic models can have errors in mean moment arm values on the order of 3 to 4 cm [30]. Similarly, errors in muscle-tendon lengths can be 10 cm or more compared to geometric data obtained from MR images [30]. Such errors have been shown to have a significant impact on predicted joint moments in an EMG-driven knee model [28]. In our study, the largest average moment arm change was 1.8 cm, while the largest average muscle-tendon length change was 3.8 cm (Tables A2 and A3). These changes are well within the error ranges reported in the literature, suggesting that the geometric adjustments were at least reasonable.

While other studies have used varied movements and dynamometer data to calibrate and test their EMG-driven models, we purposefully used only walking data combined with published passive joint moment data for our calibration process. Restoring normal walking function is a common and important clinical goal. Therefore, models that can reproduce experimental walking data have an increased likelihood of being clinically useful. Furthermore, it could be difficult in a time-limited clinical setting with function-limited patients to collect EMG, motion capture, and ground reaction data for a wide range of movement tasks. For these reasons, we decided to calibrate our EMG-driven models using only the subject's walking data and published passive joint moment data.

We made several decisions to account for the limitations of using primarily walking data for model calibration. To increase the information content in our calibration data, we used a large number of walking trials (10 per speed for either three or five speeds). As indicated by post-hoc statistical analyses, this approach resulted in joint angles, joint moments, and EMG amplitudes that were statistically different between the faster and slower walking speeds. Since walking data provide information over only limited ranges of joint motion and loading, we included published passive joint moment data [49] in our calibration process. This decision provided moment calibration information over broader ranges of motion than occur during walking. While our hemiparetic subject is likely to be less flexible than the healthy subjects used in [49], these unique data still represent the general trends in passive moments one might expect to observe in any ambulatory individual. Without including these extra data, the passive moments predicted at extreme joint angles outside the bounds of walking were unrealistic, with muscles generating passive forces that were well above maximum isometric force. Nonetheless, since our EMG-driven model calibration process was based primarily on walking data, it may not predict joint moments well for motions other than walking.

The ability of our EMG-driven model with geometric adjustments to predict joint moments well for faster non-calibration walking speeds may make this model clinically useful for predictive gait optimization studies. By incorporating our EMG-driven model into a dynamic patient-specific full-body walking model that includes deformable foot-ground contact models, researchers could predict how changes in a patient's muscle excitations could alter the patient's gait pattern in a favorable way. Muscle excitations could be controlled individually or coupled together through muscle synergies calculated from the patient's EMG data. For a subject with hemiparesis, the optimizations could seek to identify minimal changes in the patient's muscle excitations that would produce a desired improvement in walking speed and bilateral symmetry. The predicted neural control and gait pattern changes could

potentially help clinicians determine which muscles should be targeted for excitation timing changes, strength increases, and/or functional electrical stimulation (i.e., treatment prescription), as well as how much of each type of change is required (i.e., treatment dosage).

This study possesses several important limitations that have not been mentioned previously and should be considered when interpreting our results. First, due to the complexity of the EMG-driven model development process, we have only modeled a single hemiparetic subject thus far. However, the purpose of the present study was to evaluate the feasibility and potential benefits of our proposed EMG-driven modeling method with geometric adjustments, and analysis of a single subject is sufficient for those purposes. Second, our method requires EMG data, including signals from deep muscles acquired with fine-wire electrodes, for all muscles that contribute significantly to the task being modeled. In our case, this requirement meant that fine-wire data were needed from iliopsoas in particular. Without prior knowledge of muscle excitation patterns, our optimization problem would be highly underdetermined with no well-defined solution. For studies lacking critical EMG data, geometric adjustments using the methods described here would be difficult. Third, our model includes muscles for which EMG data are not available. For these muscles, we apply excitations from anatomically related muscles (review Table 1 describing how 16 EMG signals were applied to 35 muscles per leg), which may not accurately represent the true excitations. Fourth, our method used initial model parameter values and bounds taken from the literature. There is no guarantee that literature values will represent well the anatomy of a particular subject, and even using them for bounds may over-constrain the model. Unfortunately, clinical measurement of patient-specific model parameter values is not currently possible, and thus literature values must suffice as a starting point for the time being. Fifth, we assumed bilateral symmetry for most model parameter values, despite the fact that our subject had suffered a stroke. We evaluated this assumption by removing the bilateral symmetry requirement and recalibrating each leg separately across

all speeds. While this modification produced small improvements in joint moment predictions, the optimizations were more likely to get stuck in a local minimum. Furthermore, computation time increased significantly due to a near doubling in the number of model parameter values. For these reasons, we maintained bilateral symmetry for all model parameter values except excitation scale factors and time delays. For subjects with greater neurological impairment, a bilateral symmetry assumption may be more limiting.

In conclusion, the novel EMG-driven model calibration method with geometric adjustments presented in this study improved joint moment prediction accuracy for walking compared to results generated using a scaled geometric musculoskeletal model. The proposed EMG-driven model creation process can be almost entirely automated and requires little effort when compared with construction of complex geometric models from MR and/or CT data. Because of its improved moment prediction accuracy, our modeling method with geometric adjustments may prove useful in future clinical applications. Based on the results of this study, we recommend that researchers incorporate geometric adjustments into their EMG-driven modeling process to improve the accuracy of joint moment predictions for walking, especially at the hip.

References

1. Aisen ML, Kerkovich D, Mast J, Mulroy S, Wren TAL, Kay RM, et al. Cerebral palsy: clinical care and neurological rehabilitation. Lancet Neurol. 2011;10: 844–852. doi:10.1016/S1474-4422(11)70176-4

2. Feigin VL, Lawes CMM, Bennett DA, Barker-Collo SL, Parag V. Worldwide stroke incidence and early case fatality reported in 56 population-based studies: a systematic review. Lancet Neurol. 2009;8: 355–369. doi:10.1016/S1474-4422(09)70025-0

3. Soh S-E, McGinley JL, Watts JJ, Iansek R, Murphy AT, Menz HB, et al. Determinants of health-related quality of life in people with Parkinson's disease: a path analysis. Qual Life Res. 2013;22: 1543–53. doi:10.1007/s11136-012-0289-1

4. Prieto-Alhambra D, Judge A, Javaid MK, Cooper C, Diez-Perez A, Arden NK. Incidence and risk factors for clinically diagnosed knee, hip and hand osteoarthritis: influences of age, gender and osteoarthritis affecting other joints. Ann Rheum Dis. 2013; doi:10.1136/annrheumdis-2013-203355

5. Fregly BJ, Boninger ML, Reinkensmeyer DJ. Personalized neuromusculoskeletal modeling to improve treatment of mobility impairments: a perspective from European research sites. J Neuroeng Rehabil. BioMed Central; 2012;9: 18. doi:10.1186/1743-0003-9-18

6. Barrios JA, Crossley KM, Davis IS. Gait retraining to reduce the knee adduction moment through real-time visual feedback of dynamic knee alignment. J Biomech. 2010;43: 2208–13. doi:10.1016/j.jbiomech.2010.03.040

7. Mündermann A, Asay JL, Mündermann L, Andriacchi TP. Implications of increased medio-lateral trunk sway for ambulatory mechanics. J Biomech. 2008;41: 165–70. doi:10.1016/j.jbiomech.2007.07.001

8. Fregly BJ, Reinbolt JA, Rooney KL, Mitchell KH, Chmielewski TL. Design of patient-specific gait modifications for knee osteoarthritis rehabilitation. IEEE Trans Biomed Eng. 2007;54: 1687–1695. doi:10.1109/TBME.2007.891934

9. Walter JP, D'Lima DD, Colwell CW, Fregly BJ. Decreased knee adduction moment does not guarantee decreased medial contact force during gait. J Orthop Res. 2010;28: 1348–1354. doi:10.1002/jor.21142

10. Meyer AJ, D'Lima DD, Besier TF, Lloyd DG, Colwell CW, Fregly BJ. Are external knee load and EMG measures accurate indicators of internal knee contact forces during gait? J Orthop Res. 2013;31: 921–929.

11. Mulroy SJ, Klassen T, Gronley JK, Eberly VJ, Brown DA, Sullivan KJ. Gait parameters associated with responsiveness to treadmill training with body-weight support after stroke: an exploratory study. Phys Ther. 2009;90: 209–223. doi:10.2522/ptj.20090141

12. Lloyd DG, Besier TF. An EMG-driven musculoskeletal model to estimate muscle forces and knee joint moments in vivo. J Biomech. 2003;36: 765–776. doi:10.1016/S0021-9290(03)00010-1

13. Bogey RA, Perry J, Gitter AJ. An EMG-to-force processing approach for determining ankle muscle forces during normal human gait. IEEE Trans neural Syst Rehabil Eng a Publ IEEE Eng Med Biol Soc. 2005;13: 302–310. doi:10.1109/TNSRE.2005.851768

14. Sartori M, Reggiani M, Farina D, Lloyd DG. EMG-driven forward-dynamic estimation of muscle force and joint moment about multiple degrees of freedom in the human lower extremity. PLoS One. 2012;7: e52618. doi:10.1371/journal.pone.0052618

15. Kumar D, Rudolph KS, Manal KT. EMG-driven modeling approach to muscle force and joint load estimations: Case study in knee osteoarthritis. J Orthop Res. 2012;30: 377–383. doi:10.1002/jor.21544

16. Buchanan TS, Lloyd DG, Manal K, Besier TF. Estimation of muscle forces and joint moments using a forward-inverse dynamics model. Med Sci Sports Exerc. 2005;37: 1911–1916.

17. Winby CR, Lloyd DG, Besier TF, Kirk TB. Muscle and external load contribution to knee joint contact loads during normal gait. J Biomech. 2009;42: 2294–2300. doi:10.1016/j.jbiomech.2009.06.019

18. Gardinier ES, Manal K, Buchanan TS, Snyder-Mackler L. Minimum detectable change for knee joint contact force estimates using an EMG-driven model. Gait Posture. 2013;38: 1051–1053. doi:10.1016/j.gaitpost.2013.03.014

19. Gerus P, Rao G, Buchanan TS, Berton E. A clinically applicable model to estimate the opposing muscle groups contributions to isometric and dynamic tasks. Ann Biomed Eng. 2010;38: 2406–2417. doi:10.1007/s10439-010-9987-4

20. Doorenbosch CAM, Harlaar J. A clinically applicable EMG–force model to quantify active stabilization of the knee after a lesion of the anterior cruciate ligament. Clin Biomech. 2003;18: 142–149.

21. Kellis E, Baltzopoulos V. The effects of antagonist moment on the resultant knee joint moment during isokinetic testing of the knee extensors. Eur J Appl Physiol Occup Physiol. 1997;76: 253–259. doi:10.1007/s004210050244

22. Amarantini D, Martin L. A method to combine numerical optimization and EMG data for the estimation of joint moments under dynamic conditions. J Biomech. 2004;37: 1393–1404. doi:10.1016/j.jbiomech.2003.12.020

23. Liu MM, Herzog W, Savelberg HHCM. Dynamic muscle force predictions from EMG: an artificial neural network approach. J Electromyogr Kinesiol. 1999;9: 391–400. doi:10.1016/S1050-6411(99)00014-0

24. Olney SJ, Winter DA. Predictions of knee and ankle moments of force in walking from EMG and kinematic data. J Biomech. 1985;18: 9–20. doi:10.1016/0021-9290(85)90041-7

25. He J, Levine WS, Loeb GE. Feedback gains for correcting small perturbations to standing posture. IEEE Trans Automat Contr. 1991;36: 322–332. doi:10.1109/9.73565

26. Hill A V. The heat of shortening and the dynamic constants of muscle. Proc R Soc London Ser B, Biol Sci. 1938;126: 136–195. doi:10.2307/82135

27. Zajac FE. Muscle and tendon: properties, models, scaling, and application to biomechanics and motor control. Crit Rev Biomed Eng. 1989;17: 359–411.

28. Tsai L-C, Colletti PM, Powers CM. Magnetic resonance imaging-measured muscle parameters improved knee moment prediction of an EMG-driven model. Med Sci Sports Exerc. 2012;44: 305–12. doi:10.1249/MSS.0b013e31822dfdb3

29. Buchanan TS, Lloyd DG, Manal K, Besier TF. Neuromusculoskeletal modeling: estimation of muscle forces and joint moments and movements from measurements of neural command. J Appl Biomech. 2004;20: 367–395.

30. Scheys L, Spaepen A, Suetens P, Jonkers I. Calculated moment-arm and muscle-tendon lengths during gait differ substantially using MR based versus rescaled generic lower-limb musculoskeletal models. Gait Posture. 2008;28: 640–8. doi:10.1016/j.gaitpost.2008.04.010

31. Correa TA, Baker R, Graham HK, Pandy MG. Accuracy of generic musculoskeletal models in predicting the functional roles of muscles in human gait. J Biomech. 2011;44: 2096–105. doi:10.1016/j.jbiomech.2011.05.023

32. Scheys L, Van Campenhout A, Spaepen A, Suetens P, Jonkers I. Personalized MR-based musculoskeletal models compared to rescaled generic models in the presence of increased femoral anteversion: effect on hip moment arm lengths. Gait Posture. 2008;28: 358–65. doi:10.1016/j.gaitpost.2008.05.002

33. Menegaldo LL, de Toledo Fleury A, Weber HI. Moment arms and musculotendon lengths estimation for a three-dimensional lower-limb model. J Biomech. 2004;37: 1447–53. doi:10.1016/j.jbiomech.2003.12.017

34. Sartori M, Reggiani M, van den Bogert AJ, Lloyd DG. Estimation of musculotendon kinematics in large musculoskeletal models using multidimensional B-splines. J Biomech. 2012;45: 595–601. doi:10.1016/j.jbiomech.2011.10.040

35. Delp SL, Anderson FC, Arnold AS, Loan P, Habib A, John CT, et al. OpenSim: open-source software to create and analyze dynamic simulations of movement. IEEE Trans Biomed Eng. 2007;54: 1940–50. doi:10.1109/TBME.2007.901024

36. Arnold EM, Ward SR, Lieber RL, Delp SL. A model of the lower limb for analysis of human movement. Ann Biomed Eng. 2010;38: 269–79. doi:10.1007/s10439-009-9852-5

37. Reinbolt JA, Schutte JF, Fregly BJ, Koh B Il, Haftka RT, George AD, et al. Determination of patient-specific multi-joint kinematic models through two-level optimization. J Biomech. 2005;38: 621–626. doi:10.1016/j.jbiomech.2004.03.031

38. Hug F. Can muscle coordination be precisely studied by surface electromyography? J Electromyogr Kinesiol. 2011;21: 1–12. doi:10.1016/j.jelekin.2010.08.009

39. Hermens HJ, Freriks B, Disselhorst-Klug C, Rau G. Development of recommendations for SEMG sensors and sensor placement procedures. J Electromyogr Kinesiol. 2000;10: 361–374. doi:10.1016/S1050-6411(00)00027-4

40. Perotto A, Delagi EF. Anatomical guide for the electromyographer: the limbs and trunk. Charles C Thomas Publisher; 2005.

41. Delp SL, Loan JP, Hoy MG, Zajac FE, Topp EL, Rosen JM. An interactive graphics-based model of the lower extremity to study orthopaedic surgical procedures. IEEE Trans Biomed Eng. 1990;37: 757–67. doi:10.1109/10.102791

42. Manal K, Buchanan TS. A one-parameter neural activation to muscle activation model: estimating isometric joint moments from electromyograms. J Biomech. 2003;36: 1197–1202. doi:10.1016/S0021-9290(03)00152-0

43. De Groote F, Demeulenaere B, Swevers J, De Schutter J, Jonkers I. A physiology-based inverse dynamic analysis of human gait using sequential convex programming: a comparative study. Comput Methods Biomech Biomed Engin. Taylor & Francis Group; 2012;15: 1093–102. doi:10.1080/10255842.2011.571679

44. Millard M, Uchida T, Seth A, Delp SL. Flexing computational muscle: modeling and simulation of musculotendon dynamics. J Biomech Eng. American Society of Mechanical Engineers; 2013;135: 021005. doi:10.1115/1.4023390

45. Thelen DG. Adjustment of muscle mechanics model parameters to simulate dynamic contractions in older adults. J Biomech Eng. American Society of Mechanical Engineers; 2003;125: 70. doi:10.1115/1.1531112

46. An KN, Takahashi K, Harrigan TP, Chao EY. Determination of Muscle Orientations and Moment Arms. J Biomech Eng. 1984;106: 280–282. doi:10.1115/1.3138494

47. Walker PS, Rovick JS, Robertson DD. The effects of knee brace hinge design and placement on joint mechanics. J Biomech. 1988;21: 965–974. doi:10.1016/0021-9290(88)90135-2

48. Reinbolt JA, Haftka RT, Chmielewski TL, Fregly BJ. A computational framework to predict post-treatment outcome for gait-related disorders. Med Eng Phys. 2008;30: 434–443. doi:10.1016/j.medengphy.2007.05.005

49. Silder A, Whittington B, Heiderscheit B, Thelen DG. Identification of passive elastic joint moment-angle relationships in the lower extremity. J Biomech. 2007;40: 2628–35. doi:10.1016/j.jbiomech.2006.12.017

50. Handsfield GG, Meyer CH, Hart JM, Abel MF, Blemker SS. Relationships of 35 lower limb muscles to height and body mass quantified using MRI. J Biomech. 2014;47: 631–8. doi:10.1016/j.jbiomech.2013.12.002

51. Racinais S, Maf NA, Girard O. M-wave, H- and V-reflex recruitment curves during maximal voluntary contraction. J Clin Neurophysiol. 2013;30: 415–421.

52. Simonsen EB, Alkjær T, Raffalt PC. Reflex response and control of the human soleus and gastrocnemius muscles during walking and running at increasing velocity. Exp brain Res. 2012;219: 163–74. doi:10.1007/s00221-012-3075-y

53. Cronin NJ, Kumpulainen S, Joutjärvi T, Finni T, Piitulainen H. Spatial variability of muscle activity during human walking: The effects of different EMG normalization approaches. Neuroscience. 2015;300: 19–28. doi:10.1016/j.neuroscience.2015.05.003

54. Reinbolt JA, Haftka RT, Chmielewski TL, Fregly BJ. Are patient-specific joint and inertial parameters necessary for accurate inverse dynamics analyses of gait? IEEE Trans Biomed Eng. 2007;54: 782–93. doi:10.1109/TBME.2006.889187

Figure 1

Click here to download Figure Fig1 Rev1.tif

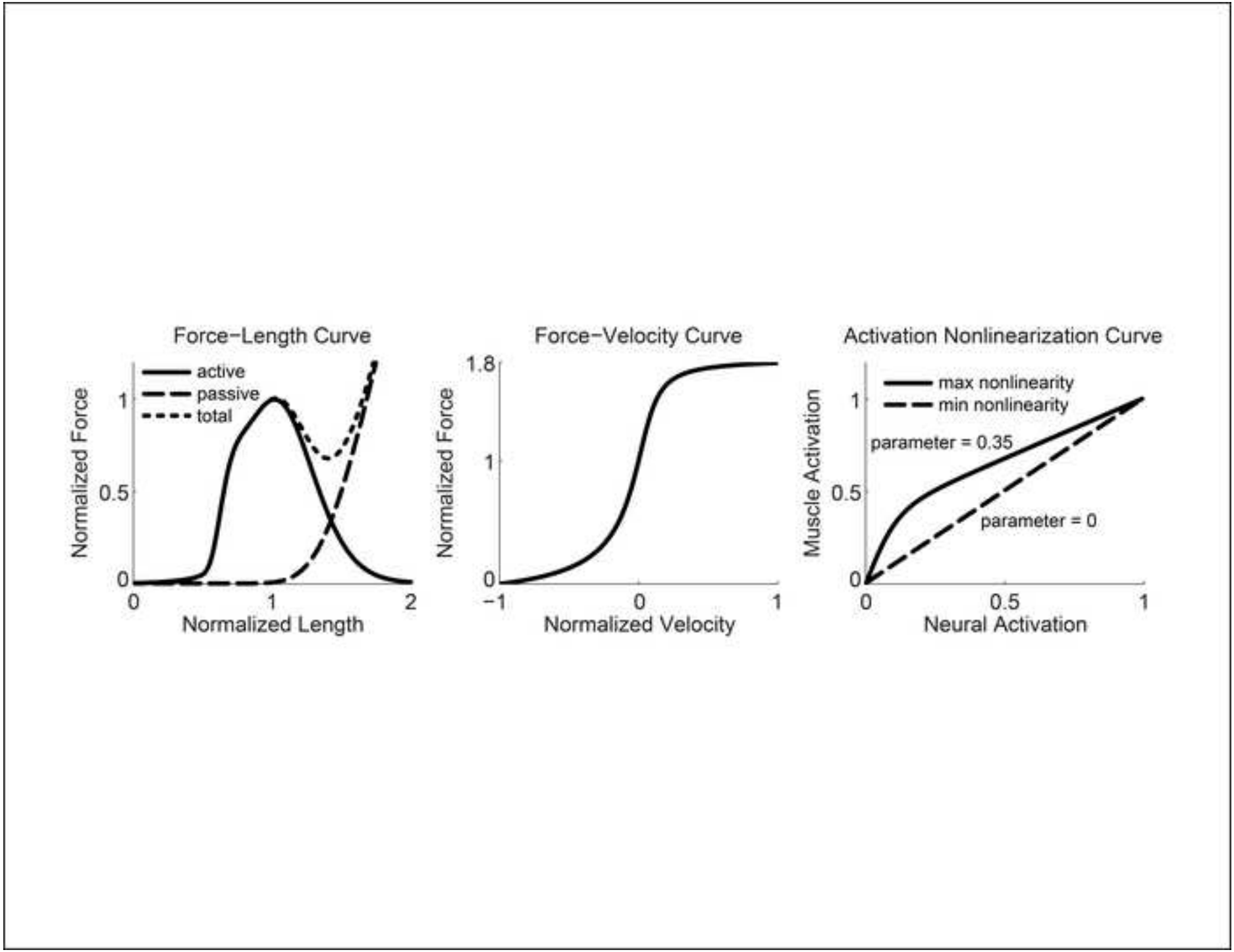

Figure 2

Click here to download Figure Fig2 Rev1.tif

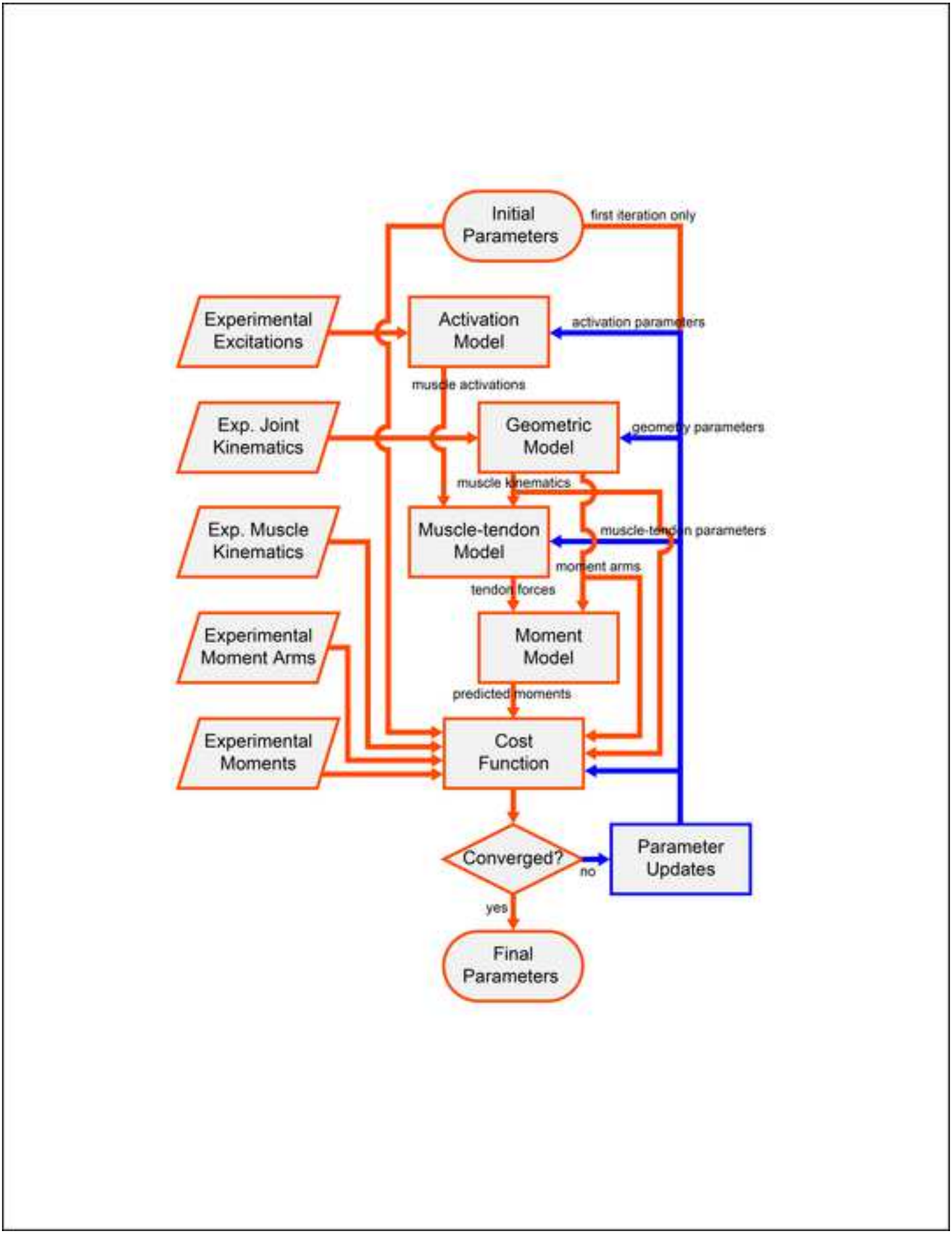

Figure 3

Click here to download Figure Fig3 Rev1.tif

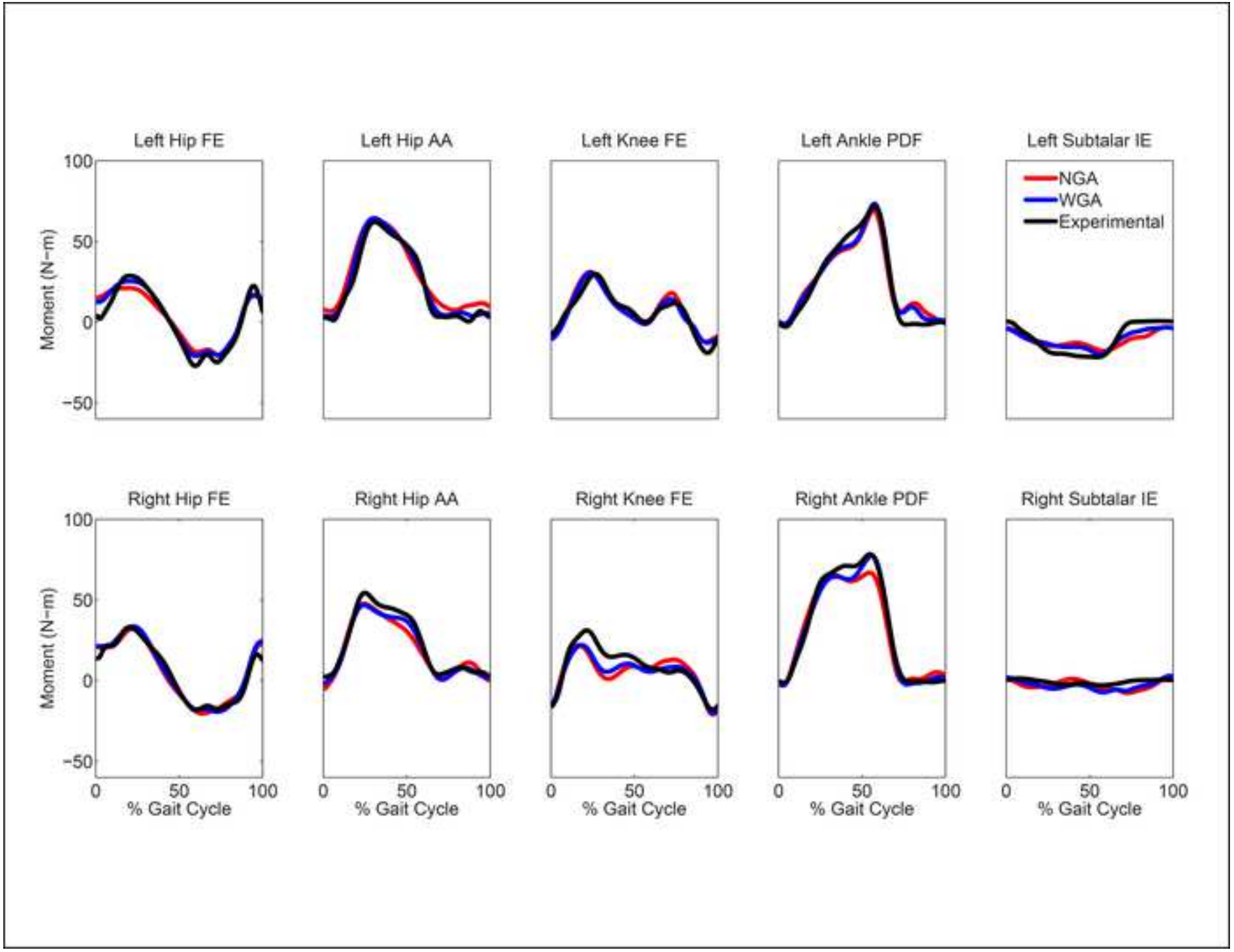

Figure 4

Click here to download Figure Fig4 Rev1.tif

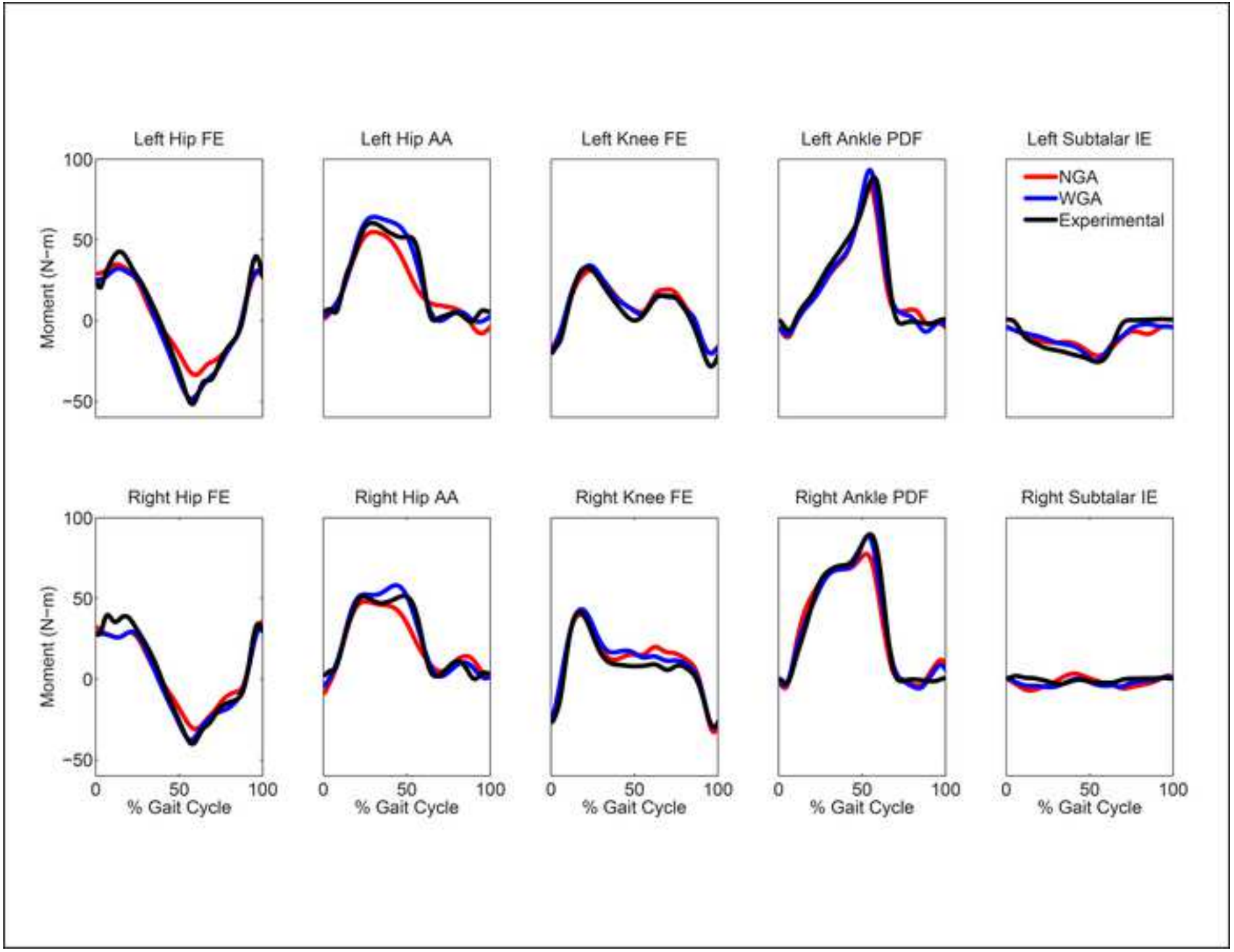

Figure 5

Click here to download Figure Fig5 Rev1.tif

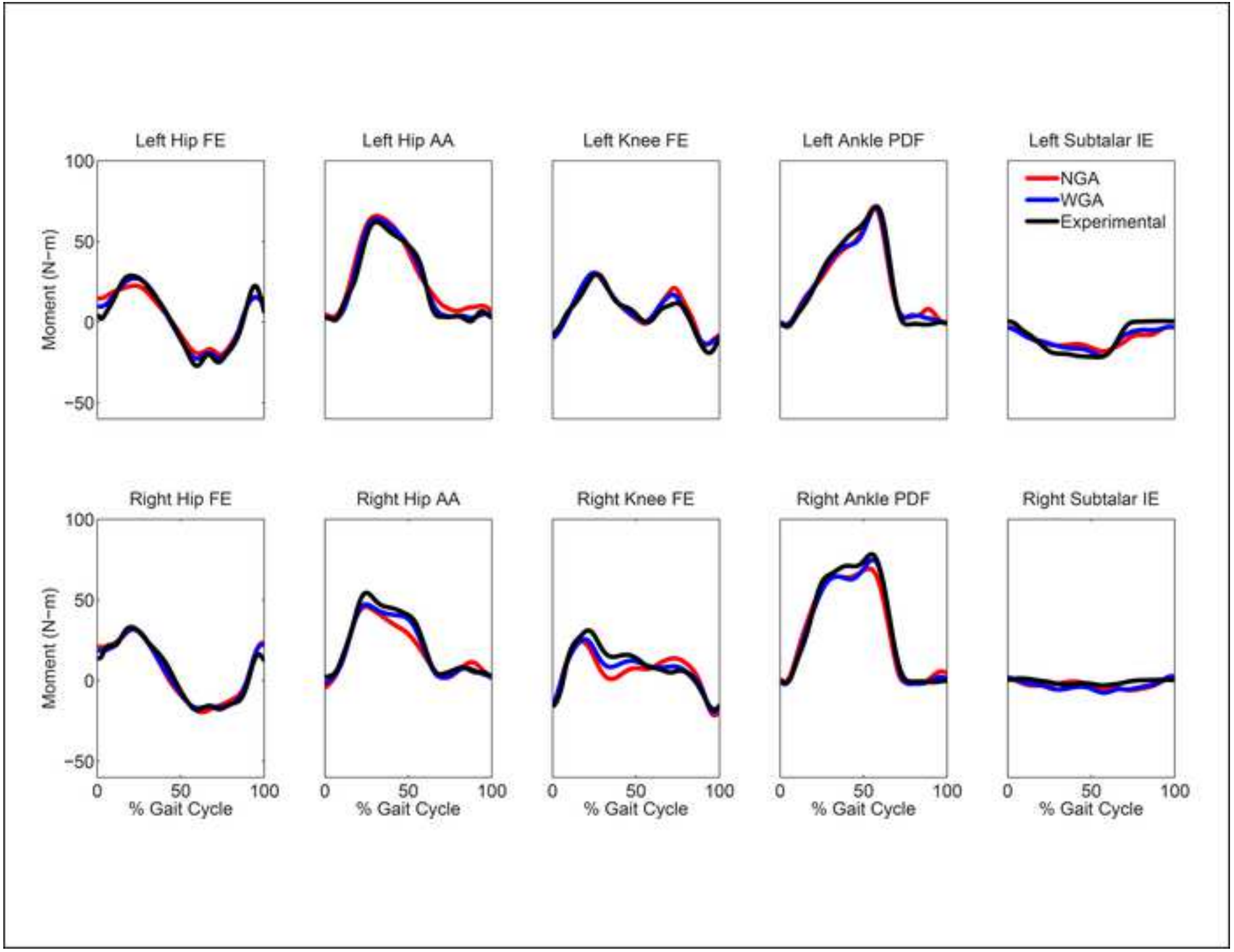

Figure 6

Click here to download Figure Fig6 Rev1.tif

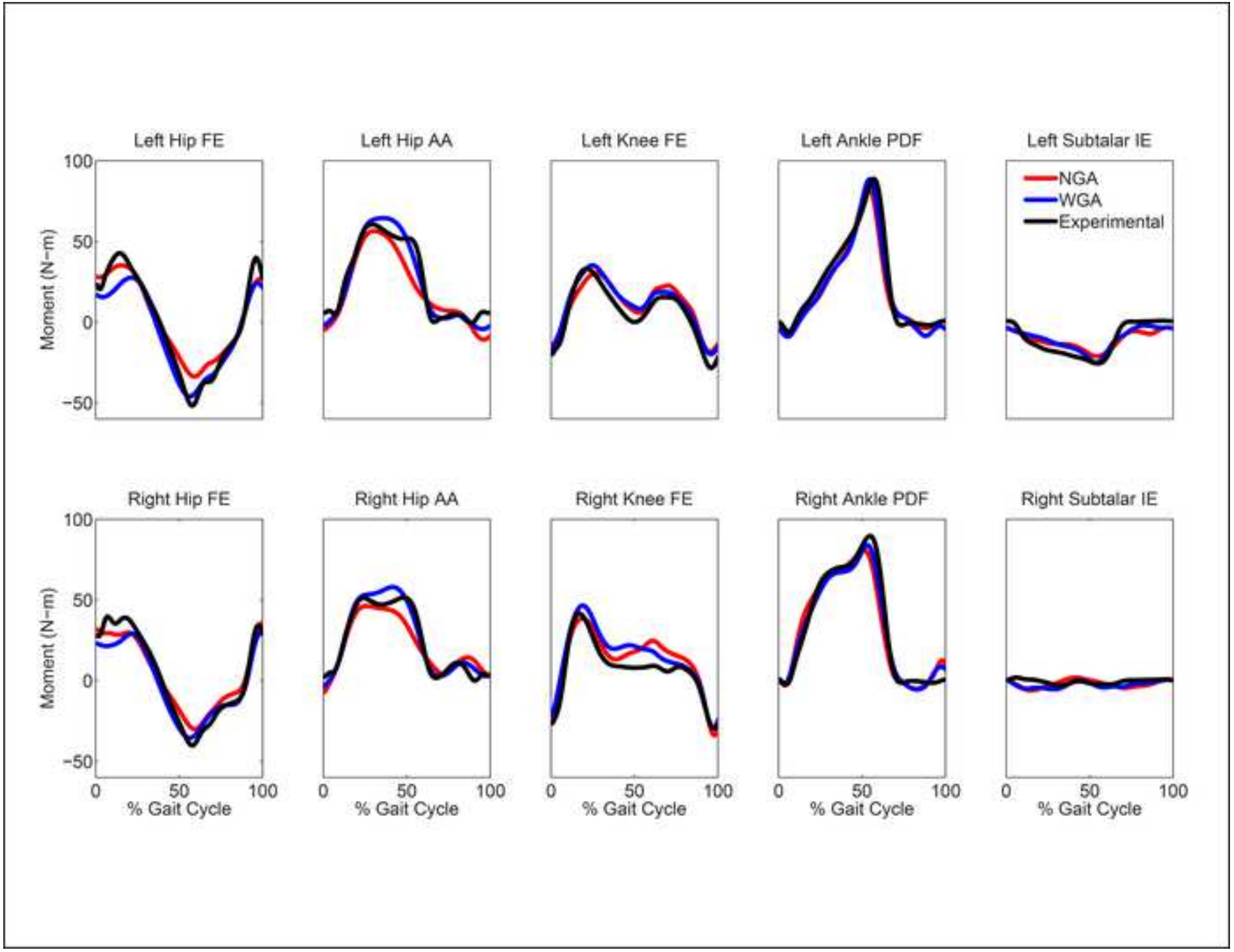

Figure 7

Click here to download Figure Fig7 Rev1.tif

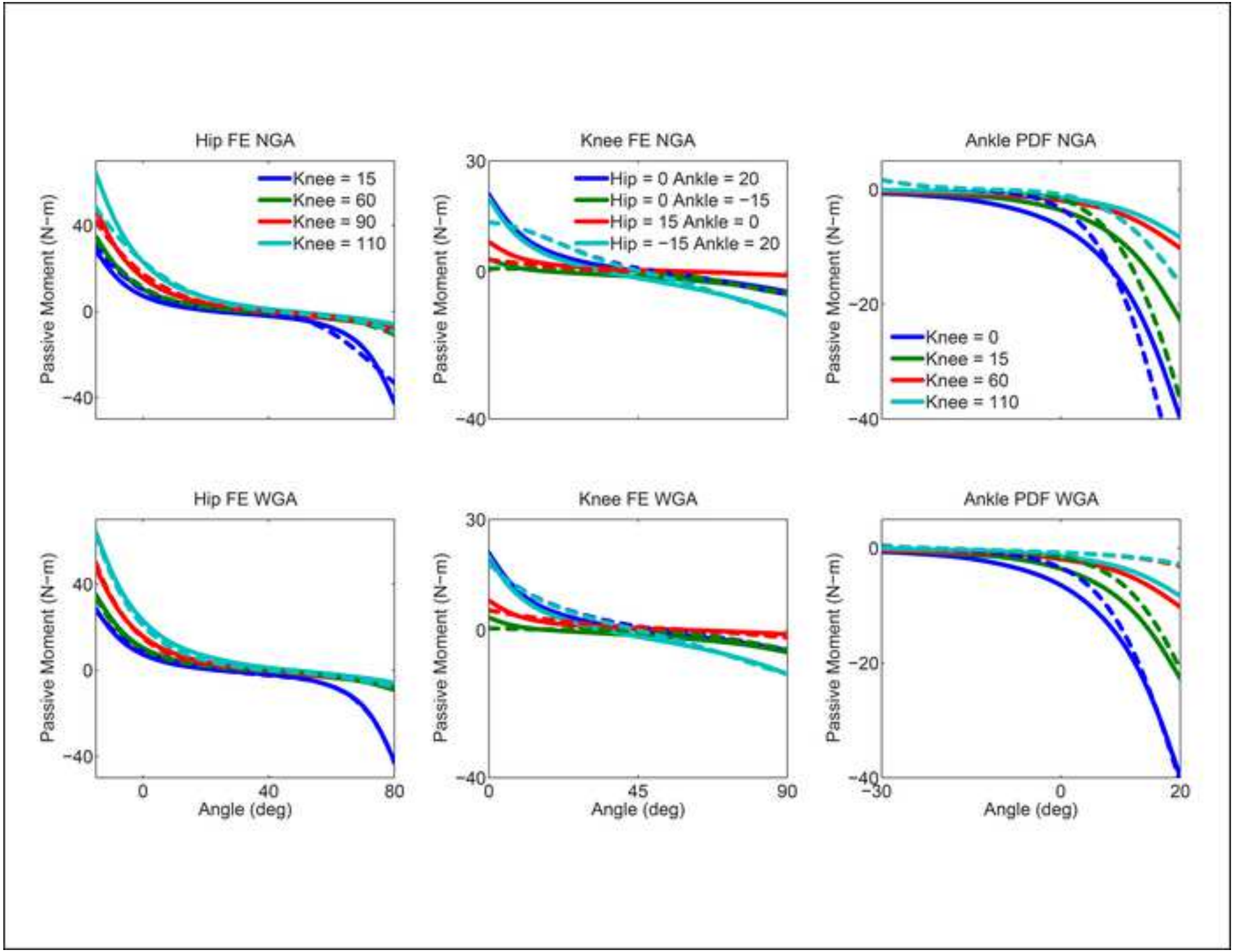

Appendix

Lower Extremity EMG-driven Modeling of Walking with Automated Adjustment of Musculoskeletal Geometry

Andrew J. Meyer[1], Carolynn Patten[2,3], and Benjamin J. Fregly[1]

[1] Department of Mechanical & Aerospace Engineering, University of Florida, Gainesville, FL

[2]Department of Physical Therapy, University of Florida, Gainesville, FL

[3]Neural Control of Movement Lab, Malcom Randall VA Medical Center, Gainesville, FL

Details of Optimization Problem Formulation

Calibration of our EMG-driven model was achieved by performing a nonlinear constrained optimization. Initial guesses, bounds, and cost function terms used in the optimization (Table 2) were specified such that the final solution would remain anatomically realistic and close to the initial model. In addition to minimizing errors in walking and passive joint moment curves, the cost function included penalty terms that acted as "soft constraints" to limit deviations of model parameter values and curves away from the initial model. Inequality "hard constraints" were also included in the problem formulation to keep normalized muscle lengths and velocities within known realistic ranges and to prevent muscle moment arms from switching signs. For each type of parameter or curve with a specified reference value and associated allowable deviation (see Table A1), a single cost function penalty term was formulated by calculating deviations of the model parameters or curves from the reference value, normalizing all deviations by the allowable deviation (which could be exceeded), and calculating the mean squared

value. For example, for shape changes in muscle-tendon length curves, there were 35 muscles per leg x 2 legs x 101 time points per gait cycle x 50 gait cycles = 530,250 shape deviation values calculated relative to reference curves from the initial model. The corresponding penalty term in the cost function was calculated by dividing each deviation value by 0.25, squaring each normalized deviation, taking the sum, and finally dividing by 530,250.

Table A1: Initial guesses, bounds, reference values, and allowable deviations for constant model parameters (top half) and time-varying model curves (bottom half). For quantities with a specified Allowable Deviation, cost function penalty terms were calculated by finding the deviation of the model parameter or curve from the specified reference value, normalizing by the allowable deviation, and calculating the mean squared value. For quantities without a specified Allowable Deviation, bounds were enforced using nonlinear inequality constraints. Surrogate geometry curves refer to muscle-tendon lengths and moment arms but not velocities. Allowable deviation values were chosen iteratively to ensure that parameter values did not change far from the reference values. Different allowable deviations were used for the hip, knee, and ankle surrogate geometry shape changes.

Model Parameter (top) or Curve (bottom)	Initial Guess	Lower Bound	Upper Bound	Reference Value	Allowable Deviation
Normalized EMG scale factor	0.25	0.05	1	1	0.5
Electromechanical delay (ms)	50	0	100	—	—
Activation time constant (ms)	15	5	35	15	15
Nonlinearity constant	0	0	0.35	0	0.25
Optimal muscle fiber length scale factor	1	0.75	1.25	1	0.15
Tendon slack length scale factor	1	0.75	1.25	1	0.15
Normalized EMG scale factor variations	—	—	—	0	1
Electromechanical delay variations (ms)	—	—	—	0	100
Normalized muscle length	—	0.3	1.3	—	—
Maximum normalized muscle length	—	0.8	—	—	—
Minimum normalized muscle length	—	—	1.0	—	—
Normalized muscle velocity	—	-1	1	—	—
Surrogate geometry mean value changes	—	—	—	0	0.5
Surrogate geometry shape changes	—	—	—	0	0.25 or 0.125
Normalized muscle length variations	—	—	—	0	1
Muscle moment arm variations (cm)	—	—	—	0	2
Inverse dynamic joint moment errors	—	—	—	0	1
Passive joint moment errors	—	—	—	0	1

Additional explanation is helpful for understanding how and why some of the design variables and their initial values and bounds were selected. Normalized processed EMG signals were multiplied by an additional scale factor to account for the fact that the maximum processed EMG value for each muscle was unlikely to be the true maximum. This decision is supported by experimental data demonstrating that the maximal M-wave is significantly larger than volitional EMG measured during walking or maximum voluntary contraction [1–3]. The upper bound for electromechanical delay was based on

values reported in the literature [4]. The initial guess of 0 for activation nonlinearity constants represents a linear relationship between neural activation and muscle activation. For surrogate geometry mean value changes (i.e., changes in mean value of a muscle-tendon length or moment arm curve), deviation was calculated as the difference in mean values between adjusted and reference curves divided by the maximum absolute value of the reference curve. For surrogate geometry shape changes (i.e., change in shape of a muscle-tendon length or moment arm curve), deviation at each time point was calculated as the difference between demeaned adjusted and reference curves divided by the range of the reference curve. For moment arm shape changes, hip moment arm deviations were normalized by 0.25 while knee and ankle moment arm deviations were normalized by 0.125 based on uncertainties reported in literature [5]. All parameter values were the same for both legs with the exception of electromechanical delays and EMG scale factors, which were specific to each muscle in each leg since the subject was hemiparetic.

Muscles that function within a physiological group or share a common EMG signal were given special treatment in the optimization cost function. For these muscles, additional "soft constraints" were included in the cost function to ensure that curves or parameter values from related muscles remained similar. For normalized EMG scale factor variations and electromechanical delay variations, deviation was calculated as the standard deviation of the scale factors or delays for all muscles in the group. For normalized muscle length variations and moment arm variations, deviation at each time point was calculated as the standard deviation of the lengths or moments arms for all muscles in the group.

Determination of appropriate initial values for optimal muscle fiber lengths and tendon slack lengths required additional steps. Initial values taken from the literature [6] produced excessively high or low normalized muscle lengths for some muscles. Excessively high normalized muscle lengths produce unrealistically high passive joint moments, while excessively low normalized muscle lengths cause

muscles to produce little force even when fully activated. To address this issue, we performed a preliminary optimization to determine initial values of optimal muscle fiber lengths and tendon slack lengths that placed every muscle within a physiological operating range over the gait cycle [7]. The optimization cost function minimized changes in initial parameter values taken from the literature while also minimizing errors in model-predicted passive joint moments relative to experimental curves reported in the literature [8]. Exponential terms were also included in the cost function to limit normalized muscle lengths during walking to between 0.3 and 1.3 [7]. The pre-optimized optimal muscle fiber length and tendon slack length values were used in the larger EMG-driven calibration process.

Three categories of model parameter values were unaltered during the calibration process. For the activation model, the deactivation time constant for each muscle was specified to be four times the muscle's activation time constant. For the Hill-type muscle model, peak isometric force were calculated using regression equations reported in literature [9], with a muscle specific tension of 61 N/cm^2 [6]. Pennation angles were taken from the initial model [6]. Since muscle excitations were scaled during the EMG-driven model calibration process, adjustment of peak isometric force and pennation angle values would have been redundant since all three quantities scale the muscle force in the Hill-type model equations.

Details of Outlier Identification Methods

Given the curves output by OpenSim analyses, we performed a series of tests to identify and remove outlier trials and select trials for use in calibration and testing. First, for trials of the same speed, any gait cycle where a muscle's peak EMG value was greater than three times its median peak value was removed from the data set. Next, for each walking speed, any trial with a joint moment, angle, angular

velocity, or moment arm curve more than five standard deviations away from its mean curve at any point in the gait cycle was removed from the data set. Once outlier trials were identified and removed, calibration and testing trials were selected from the remaining trials. For each gait speed, 20 of the remaining trials were selected for subsequent analysis - ten for calibration and ten for testing.

Tables of Muscle-tendon Length and Moment Arm Changes

The tables below provide quantitative information on how muscle-tendon lengths and moment arms were changed for the EMG-drive model calibration process with geometric adjustments when data from all five walking speeds were used for calibration (Table A2) and when data from only the three slowest walking speeds were used for calibration (Table A3).

Table A2: Mean changes in muscle-tendon lengths and moment arms for calibration walking trials from a model calibration performed using data from all walking speeds. Percent changes were calculated using each curve's maximum absolute value.

	ℓ^{MT}		Hip FE		Hip AA		Knee FE		Ankle PDF		Ankle IE	
Muscle	cm	%	cm	%	cm	%	cm	%	cm	%	cm	%
Adductor brevis	2.30	15.12	0.04	1.05	0.04	0.50	--	--	--	--	--	--
Adductor longus	0.34	1.39	0.71	11.66	1.67	20.96	--	--	--	--	--	--
Adductor magnus distal	1.78	7.15	0.48	9.46	0.04	0.73	--	--	--	--	--	--
Adductor magnus ischial	1.68	4.56	0.05	0.70	0.09	1.80	--	--	--	--	--	--
Adductor magnus middle	1.12	6.93	0.76	29.62	0.13	1.86	--	--	--	--	--	--
Adductor magnus proximal	1.18	9.31	0.16	5.62	0.05	0.81	--	--	--	--	--	--
Gluteus maximus superior	1.33	5.80	0.27	4.62	0.69	21.86	--	--	--	--	--	--
Gluteus maximus middle	0.85	3.19	0.64	9.15	0.57	25.35	--	--	--	--	--	--
Gluteus maximus inferior	0.89	3.07	0.83	9.26	0.89	17.53	--	--	--	--	--	--
Gluteus medius anterior	0.40	3.00	0.99	30.62	1.72	36.69	--	--	--	--	--	--
Gluteus medius middle	0.63	4.35	0.69	18.09	0.46	10.82	--	--	--	--	--	--
Gluteus medius posterior	0.88	6.60	0.65	17.26	0.94	23.90	--	--	--	--	--	--
Gluteus minimus anterior	1.41	16.08	0.23	11.57	0.22	4.80	--	--	--	--	--	--
Gluteus minimus middle	1.71	19.31	0.95	39.83	0.17	3.70	--	--	--	--	--	--
Gluteus minimus posterior	0.58	6.05	0.67	24.40	0.10	2.48	--	--	--	--	--	--
Iliacus	2.17	9.69	0.33	7.40	0.65	67.63	--	--	--	--	--	--
Psoas	1.56	6.54	0.40	12.32	0.23	18.25	--	--	--	--	--	--
Semimembranosus	0.73	1.74	0.41	6.40	0.42	17.90	0.41	8.19	--	--	--	--
Semitendinosus	3.46	7.35	0.83	10.90	1.10	29.65	0.41	6.98	--	--	--	--

Biceps femoris long head	0.60	1.41	0.19	2.58	1.78	53.88	0.62	15.27	--	--	--	--
Biceps femoris short head	1.03	4.51	--	--	--	--	0.18	4.38	--	--	--	--
Rectus femoris	0.76	1.80	0.74	13.25	1.73	71.85	0.78	16.60	--	--	--	--
Vastus medialis	0.07	0.35	--	--	--	--	0.27	6.46	--	--	--	--
Vastus lateralis	1.03	4.34	--	--	--	--	0.35	8.23	--	--	--	--
Vastus intermedius	0.92	4.13	--	--	--	--	0.37	8.52	--	--	--	--
Lateral gastrocnemius	0.20	0.39	--	--	--	--	0.35	13.86	0.43	9.87	0.24	27.90
Medial gastrocnemius	0.26	0.52	--	--	--	--	0.25	8.13	0.41	9.55	0.64	91.89
Tibialis anterior	0.25	0.77	--	--	--	--	--	--	0.05	0.99	0.52	42.32
Tibialis posterior	0.02	0.05	--	--	--	--	--	--	0.21	23.30	0.11	6.37
Peroneus tertius	0.41	1.92	--	--	--	--	--	--	0.48	66.66	0.28	9.32
Peroneus longus	0.10	0.25	--	--	--	--	--	--	0.15	15.28	0.13	4.70
Peroneus tertius	0.20	1.03	--	--	--	--	--	--	0.20	6.45	0.65	27.08
Soleus	0.13	0.35	--	--	--	--	--	--	1.83	43.99	0.16	20.59
Extensor digitorum longus	0.04	0.09	--	--	--	--	--	--	0.05	1.33	0.05	3.06
Flexor digitorum longus	0.02	0.04	--	--	--	--	--	--	0.01	0.95	0.13	7.75
Max Change	3.46	19.31	0.99	39.83	1.78	71.85	0.78	16.60	1.83	66.66	0.65	91.89

1

Table A3: Mean changes in muscle-tendon lengths and moment arms for calibration walking trials from a model calibration performed using data from only the three slowest speeds. Percent changes were calculated with respect to each curve's maximum absolute value.

	ℓ^{MT}		Hip FE		Hip AA		Knee FE		Ankle PDF		Ankle IE	
Muscle	cm	%	cm	%	cm	%	cm	%	cm	%	cm	%
Adductor brevis	2.54	17.08	0.04	0.88	0.06	0.79	--	--	--	--	--	--
Adductor longus	1.05	4.32	0.12	2.02	0.17	2.19	--	--	--	--	--	--
Adductor magnus distal	1.20	4.88	0.31	6.01	0.17	2.96	--	--	--	--	--	--
Adductor magnus ischial	0.66	1.82	0.16	2.42	0.08	1.71	--	--	--	--	--	--
Adductor magnus middle	1.42	8.88	0.41	16.86	0.05	0.80	--	--	--	--	--	--
Adductor magnus proximal	0.55	4.44	1.59	56.89	0.93	15.25	--	--	--	--	--	--
Gluteus maximus superior	1.14	4.97	0.12	2.13	0.51	17.47	--	--	--	--	--	--
Gluteus maximus middle	0.84	3.17	0.39	5.63	0.44	21.33	--	--	--	--	--	--
Gluteus maximus inferior	0.43	1.52	0.42	4.69	0.54	11.29	--	--	--	--	--	--
Gluteus medius anterior	1.65	12.42	0.91	28.53	0.89	19.07	--	--	--	--	--	--
Gluteus medius middle	0.22	1.52	0.45	11.70	0.50	11.76	--	--	--	--	--	--
Gluteus medius posterior	0.16	1.21	0.40	11.00	1.24	31.49	--	--	--	--	--	--
Gluteus minimus anterior	0.71	8.05	0.34	17.45	0.21	4.62	--	--	--	--	--	--
Gluteus minimus middle	0.58	6.55	0.45	18.86	0.14	3.07	--	--	--	--	--	--
Gluteus minimus posterior	0.54	5.62	0.58	21.37	0.10	2.52	--	--	--	--	--	--
Iliacus	1.44	6.48	0.26	5.90	0.57	74.82	--	--	--	--	--	--
Psoas	1.10	4.64	0.07	2.10	0.25	22.28	--	--	--	--	--	--
Semimembranosus	0.83	2.01	0.33	5.12	0.30	13.47	0.49	9.93	--	--	--	--
Semitendinosus	3.82	8.26	0.39	5.20	0.82	23.28	0.33	5.53	--	--	--	--

Biceps femoris long head	0.38	0.91	0.18	2.47	0.71	23.11	0.72	17.72	--	--	--	--
Biceps femoris short head	0.93	4.09	--	--	--	--	0.05	1.11	--	--	--	--
Rectus femoris	0.80	1.91	0.65	11.77	0.92	40.47	0.66	14.12	--	--	--	--
Vastus medialis	0.72	3.44	--	--	--	--	0.19	4.51	--	--	--	--
Vastus lateralis	1.62	6.87	--	--	--	--	0.25	5.94	--	--	--	--
Vastus intermedius	1.24	5.63	--	--	--	--	0.29	6.67	--	--	--	--
Lateral gastrocnemius	0.25	0.49	--	--	--	--	0.31	12.21	0.73	16.92	0.66	75.61
Medial gastrocnemius	0.28	0.56	--	--	--	--	1.02	34.22	0.58	13.64	0.83	120.54
Tibialis anterior	0.19	0.57	--	--	--	--	--	--	0.06	1.27	0.37	30.11
Tibialis posterior	0.01	0.04	--	--	--	--	--	--	0.19	21.19	0.11	6.20
Peroneus tertius	0.20	0.92	--	--	--	--	--	--	0.36	51.04	0.20	6.51
Peroneus longus	0.08	0.19	--	--	--	--	--	--	0.08	8.05	0.07	2.70
Peroneus tertius	0.22	1.12	--	--	--	--	--	--	0.16	5.29	0.73	30.38
Soleus	0.10	0.28	--	--	--	--	--	--	1.62	39.17	0.12	15.10
Extensor digitorum longus	0.01	0.02	--	--	--	--	--	--	0.05	1.21	0.07	4.70
Flexor digitorum longus	0.02	0.05	--	--	--	--	--	--	0.06	7.27	0.04	2.27
Max Change	3.82	17.08	1.59	56.89	1.24	74.82	1.02	34.22	1.62	51.04	0.83	120.54

References

1. Racinais S, Maf NA, Girard O. M-wave, H- and V-Reflex Recruitment Curves During Maximal Voluntary Contraction. J Clin Neurophysiol. 2013;30: 415–421.
2. Cronin NJ, Kumpulainen S, Joutjärvi T, Finni T, Piitulainen H. Spatial variability of muscle activity during human walking: The effects of different EMG normalization approaches. Neuroscience. 2015;300: 19–28. doi:10.1016/j.neuroscience.2015.05.003
3. Simonsen EB, Alkjær T, Raffalt PC. Reflex response and control of the human soleus and gastrocnemius muscles during walking and running at increasing velocity. Exp brain Res. 2012;219: 163–74. doi:10.1007/s00221-012-3075-y
4. Sartori M, Reggiani M, Farina D, Lloyd DG. EMG-Driven Forward-Dynamic Estimation of Muscle Force and Joint Moment about Multiple Degrees of Freedom in the Human Lower Extremity. PLoS One. 2012;7: e52618. doi:10.1371/journal.pone.0052618

5. Scheys L, Van Campenhout A, Spaepen A, Suetens P, Jonkers I. Personalized MR-based musculoskeletal models compared to rescaled generic models in the presence of increased femoral anteversion: effect on hip moment arm lengths. Gait Posture. 2008;28: 358–65. doi:10.1016/j.gaitpost.2008.05.002
6. Arnold EM, Ward SR, Lieber RL, Delp SL. A model of the lower limb for analysis of human movement. Ann Biomed Eng. 2010;38: 269–79. doi:10.1007/s10439-009-9852-5
7. Arnold EM, Delp SL. Fibre operating lengths of human lower limb muscles during walking. Philos Trans R Soc Lond B Biol Sci. 2011;366: 1530–9. doi:10.1098/rstb.2010.0345
8. Silder A, Whittington B, Heiderscheit B, Thelen DG. Identification of passive elastic joint moment-angle relationships in the lower extremity. J Biomech. 2007;40: 2628–35. doi:10.1016/j.jbiomech.2006.12.017
9. Handsfield GG, Meyer CH, Hart JM, Abel MF, Blemker SS. Relationships of 35 lower limb muscles to height and body mass quantified using MRI. J Biomech. 2014;47: 631–8. doi:10.1016/j.jbiomech.2013.12.002